communications biology

A Nature Portfolio journal

Article

https://doi.org/10.1038/s42003-025-07836-z

Maternal high-fat diet disrupts intestinal mucus barrier of offspring by regulating gut immune receptor LRRC19

Yue Sun[1,2,4], Shumin Huang[1,4], Mengfan Li[1,4], Yunwei Yang[1,4], Jiahui Ma[1], Runxiang Xie[1], Jingyi Wang[1], Qianjing Zhao[1], Siqi Qin[1], Linlin He[1], Jiaying Jiang[1], Qing Zhao[1], Ge Jin[1], Xiang Liu[1], Huan Huang[1], Yazheng Yang[3], Jianmei Wei[3], Wentian Liu[1], Bangmao Wang[1], Rongcun Yang[3], Xiaomin Su[3,5] ✉ & Hailong Cao[1,5] ✉

Maternal high fat diet (MHFD) increased colitis susceptibility in adulthood. However, the mechanism remains unclear. We sought to explore whether novel gut immune receptor leucine-rich repeat C19 (LRRC19) contributed to the impaired mucus barrier of offspring exposed to MHFD via gut immune response and microbiota. The results showed that MHFD significantly impaired the intestinal mucus barrier of offspring, and up-regulated the expression of LRRC19. *Lrrc19* deletion alleviated the mucus barrier disruption. Mechanistically, metagenome sequencing revealed that the MHFD-induced gut microbiota alteration was partly restored in *Lrrc19*$^{-/-}$ offspring. Muc2-associated bacteria were decreased in the MHFD group, such as *Akkermansia_muciniphila_CAG_154*, which increased in the *Lrrc19*-deficient offspring. Moreover, *Lrrc19*$^{-/-}$ offspring had a higher rate of indole-3-acetic acid (IAA)-producing bacterium, such as *Lactobacillus reuteri*. A targeted metabolomics analysis revealed that IAA emerged as the top candidate that might mediate the protective effects. IAA was found to improve the mucus barrier function by increasing the ratio of interleukin-22 (IL-22)$^{+}$ ILC3 cells in an aryl hydrocarbon receptor (AhR)-dependent manner. These results suggest that MHFD disrupts the intestinal mucus barrier of offspring through regulating gut immune receptor LRRC19 and inducing an imbalance of gut microbiota and microbiota-derived metabolites.

The neonatal window was first highlighted by epidemiological studies, which revealed the pivotal role of the early life stage in gut bacterial colonization and immune development. Early-life microbial colonization has profound influences on immunological development and further enhances the immune-related disease susceptibility. The early life stage thus is a vital "window of opportunity"[1,2]. Early-life events such as maternal high-fat diet (MHFD) and antibiotic application are considered to be influential factors for gut dysbiosis in offspring by affecting the establishment of microbiome. Early life events cause permanent adverse outcomes in later life like the development of inflammatory bowel disease, allergy, asthma, obesity, and mental illness[3–7]. Particularly, several studies reported that MHFD during gestation and lactation induces the change of gut microbial structure in rodent and primate models, and these effects may predispose the offspring to various sicknesses (for example, non-alcoholic liver disease, neurodevelopmental disorders, cardiovascular diseases, colitis, and so on)[8–10]. Consistently, our previous study suggested that MHFD can damage the gut mucus barrier, drive dysbiosis and intestinal low-grade inflammation in offspring, and further enhance colitis sensitivity in adulthood[11]. However, involving mechanisms of how MHFD disrupted the intestinal mucus barrier remain unknown.

Studies have provided evidence that microorganisms colonization in early life can modulate the establishment of mucosal innate immunity and the maturation of adaptive immunity in germ-free animals[1]. Several leucine-rich repeat (LRR) proteins, like toll-like protein receptors (TLRs) and nod-like protein receptors (NLRs), exert a major influence on maintaining host homeostasis by participating in many biological processes, including

[1]Department of Gastroenterology and Hepatology, Tianjin Medical University General Hospital, Tianjin Key Medical Discipline (Specialty), Tianjin Institute of Digestive Diseases, Tianjin Key Laboratory of Digestive Diseases, Tianjin, 300052, China. [2]Department of Endoscopy, Guangdong Provincial People's Hospital (Guangdong Academy of Medical Sciences), Southern Medical University, Guangzhou, 510080, China. [3]Department of Immunology, Nankai University School of Medicine, Nankai University, Tianjin, 300071, China. [4]These authors contributed equally: Yue Sun, Shumin Huang, Mengfan Li, Yunwei Yang. [5]These authors jointly supervised this work: Xiaomin Su, Hailong Cao. ✉e-mail: xiaominsu@nankai.edu.cn; caohailong@tmu.edu.cn

pathogen recognition, immune response, cell adhesion, and signaling[12]. Interestingly, immune receptors could also impact the intestinal microbiota composition in turn. Previous studies have suggested that TLR5 might function by recognizing and responding to the flagellated pathogen, and substantially influence microbiota composition. *Tlr5* deficiency during the neonatal period could result in a high abundance of flagellated bacteria and an alteration of the microbiota, leading to metabolic or immunological consequences[13]. In addition, intestinal epithelial TLR4 could prevent metabolic syndrome by influencing the structure of gut microbiota and its communication with intestinal epithelial cells[14]. These studies demonstrated the important value of the interaction between microbiota and immunoreceptors on host-microbiota homeostasis. As a novel gut epithelial receptor differs from other pathogen-recognizing receptors, leucine-rich repeat C19 (LRRC19) can trigger NF-κB activation and facilitate the expression of proinflammatory genes regardless of the presence of TLR ligands. Under normal physiological conditions, intestinal epithelial cells exhibit high expression of LRRC19. Our previous study has found that LRRC19 involves the identification of pathogenic microorganisms, and affects the gut immune system as well as the intestinal inflammation responses. Moreover, the gut microbiota composition in the *Lrrc19*$^{-/-}$ mice was altered compared to the cohoused wild type (*Lrrc19*$^{+/+}$) mice, and *Lrrc19* deficiency not only impaired intestinal immune responses but also reduced the gut inflammatory reactions[15–17].

Multiple researches revealed that intestinal microbiota could strongly affect the establishment of the host immune system as well as the intestinal mucosal barrier[18,19]. The gut mucosal barrier is composed of immunological and biochemical components and functions as host's first line to resist against pathogens; the disruption of intestinal mucosal barrier can provoke immune responses and is involved in the occurrence of many chronic diseases[20]. Specifically, the intestinal mucus layer, which is a highly ordered glycoprotein network (primarily composed of MUC2 which are complex agglomerates of heavily O-glycosylated or fucosylated proteins) contributed by goblet cells, has a pivotal regulatory function in the interaction with gut microbiota and contributes to the protection of intestine[21]. Previous work demonstrated that the gut epithelial receptors, including TLRs, exert pivotal effects in mucosal immune defense through recognizing the microbiota and metabolites[22]. Moreover, microbial metabolites could regulate the colonization of microbiota and maintain the homeostasis of intestinal epithelium[23]. Meanwhile, our recent study has indicated that LRRC19 can lead to increased intestinal permeability, and a tighter junction between colonic cells was observed under *Lrrc19*-deficient background[24]. These studies emphasized the importance of microbiota and bacterial metabolites in maintaining epithelial function. Given these, we hypothesized that LRRC19 could be involved in the MHFD-induced impaired intestinal mucus barrier of the offspring.

Here we investigated the impact of LRRC19 on MHFD-induced intestinal microbiota alteration and intestinal mucus barrier disruption. Our experiments revealed that MHFD decreased the production and fucosylation of MUC2, impaired the intestinal mucus barrier function, and upregulated the expression of LRRC19 in offspring; in contrast, LRRC19 depletion alleviated the destruction of the gut mucus barrier in offspring exposed to MHFD, and partly reversed the alteration of gut microbiota and modulated the tryptophan metabolism of offspring. These findings revealed that LRRC19 might have a critical role in disrupting gut mucus barrier function by involving in the gut microbiota alteration and microbial metabolism when exposed to MHFD. Therefore, this work provided a novel perspective for understanding the intricate interaction among maternal western diet, gut immune receptor, and gut microbial metabolism.

Results

MHFD inhibited the intestinal development and goblet cell differentiation of offspring mice

We found that the body weight of 3-week-old offspring in MHFD group was significantly increased compared with that in MCD group (Fig. 1A). To evaluate the gut development of 3-week-old offspring in both groups, the length of villi in small intestinal tissue and depth of crypts in colonic tissue were measured (Fig. 1C and D). The length of villi and depth of crypts in MHFD group were significantly decreased than those in MCD group as shown. Meanwhile, the proliferation of intestinal cells in pups was quantified by Ki-67 staining. Compared with the MCD group, the MHFD group showed a decrease in Ki-67 positive cells (Fig. 1E). Moreover, the number of goblet cells in each crypt was significantly decreased in MHFD group as indicated by PAS staining (Fig. 2A). Collectively, these results suggest that MHFD can suppress the development and cellular differentiation of the offspring intestinal tract.

MHFD impaired the intestinal mucus barrier and increased LRRC19 expression in offspring

Goblet cells are differentiated from intestinal epithelium and are involved in the production and storage of MUC2, which acts as a primary component of the mucus layer (the extracellular components of the anatomic barrier)[25]. In this study, a significant decrease of MUC2-positive cells in each crypt was observed in MHFD group (Fig. 2B). Moreover, the number of MUC2^{+}UEA-I^{+} goblet cells in the colon mucosa in MHFD offspring decreased, implicating a decrease of mucin fucosylation (Supplementary Fig. 1A and B). Consistently, a decreased expression of *Muc2* in mRNA levels was detected in MHFD group (Fig. 2C). Furthermore, the immunostaining of IgA, which is crucial to maintaining gut immunological homeostasis, was performed[26]. A significant reduction of IgA levels in the small intestine was observed in MHFD group (Supplementary Fig. 1C). Compared with the MCD group, the MHFD group showed an increased expression of LRRC19 (Fig. 2D). These data collectively demonstrate that MHFD can impair the intestinal mucus barrier and increase LRRC19 expression in offspring.

LRRC19 depletion alleviated intestinal mucus barrier disruption of offspring exposed to MHFD

In order to further verify the effect of LRRC19 and explored the mechanism of MHFD-induced intestinal mucus barrier disruption, we established the *Lrrc19*$^{-/-}$ mice model to investigate the intestinal mucus barrier function between the *Lrrc19*$^{+/+}$ offspring and the *Lrrc19*$^{-/-}$ offspring with the damaging factor of MHFD. No difference was found in the body weight of 3-week-old offspring between the WT-MHFD group and *Lrrc19*$^{-/-}$-MHFD group (Fig. 3C). However, significant increases of the length of villi and depth of crypts were observed in *Lrrc19*$^{-/-}$-MHFD group (Fig. 3D and E). Meanwhile, compared with the WT-MHFD group, the *Lrrc19*$^{-/-}$-MHFD group showed an increase of the number of goblet cells in each crypt (Fig. 4A and B). Collectively, these results suggest that LRRC19 depletion could improve intestinal development and goblet cell differentiation of offspring in MHFD model, and these effects might be independent of body weight.

Subsequently, the production and fucosylation of MUC2 were detected in the WT-MHFD group and *Lrrc19*$^{-/-}$-MHFD group. A significant increase of the number of MUC2 positive cells in each crypt was found in *Lrrc19*$^{-/-}$-MHFD group by immunohistochemical staining (Fig. 4B). In parallel, an increased expression of *Muc2* in mRNA levels was detected in *Lrrc19*$^{-/-}$-MHFD group (Fig. 4C). Moreover, an increased number of MUC2^{+}UEA-I^{+} goblet cells in the colonic mucosa of offspring in the *Lrrc19*$^{-/-}$-MHFD group was shown, implicating an increase in mucin fucosylation (Supplementary Fig. 2A and B). In addition, immunostaining of IgA showed LRRC19 depletion significantly increased the level of IgA in the small intestine (Supplementary Fig. 2C). A decreased IL-22 production was observed in MHFD group compared to the MCD group, while *Lrrc19* deficiency reversed IL-22 expression in the high-fat diet compared to WT mice (Fig. 4D and E). Thus, these data indicate that LRRC19 depletion can promote the production and fucosylation of MUC2 and alleviate MHFD-induced intestinal mucus barrier disruption of offspring.

Furthermore, we investigated intestinal growth and differentiation of the 3-week-old *Lrrc19*$^{-/-}$ mice and *Lrrc19*$^{+/+}$ mice under MCD background. No significant differences were observed in the ileum villus length and colon crypts depth between the WT-MCD group and *Lrrc19*$^{-/-}$-MCD group

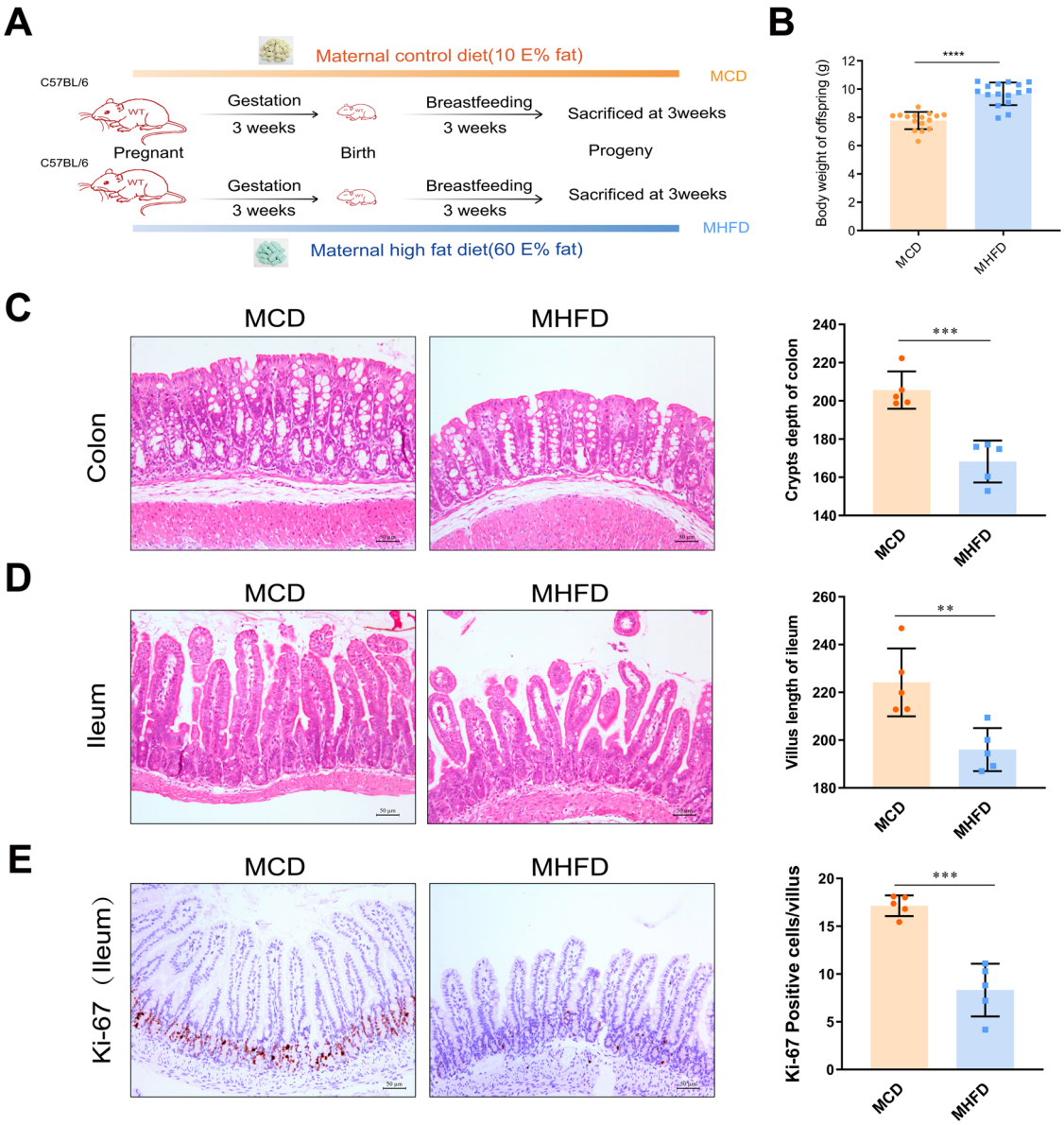

Fig. 1 | Maternal high-fat diet disrupts intestinal development and intestinal barrier in offspring. A Experimental flow diagram of MCD and MHFD groups. C57BL/6 female mice were fed either a control or a high-fat diet constantly during the gestation and lactation periods as described. Pups were sacrificed after weaning at 3 weeks old. **B** Body weight of 3-week-old pups. $n = 16$ per group. **C** Haematoxylin and eosin (H&E) staining of colonic tissues in the 3-week-old offspring between two groups. Five random fields from ×200 images were viewed for each mouse and the depth of well-orientated crypts was measured. Scale bar = 50 μm. The crypts depth of colon in both groups was counted. $n = 5$ mice per group. **D** H&E staining of small intestinal tissues and the villus length of ileum in the 3-week-old offspring in MCD, MHFD groups. Five random fields from ×200 images were viewed for each mouse and the length of well-orientated villi was measured. $n = 5$ mice per group. Scale bar = 50 μm. **E** Intestinal proliferation was assessed by Ki-67 immunostaining of ileum tissue. The number of positively stained cells in each villus of five random fields from ×200 images was counted. $n = 5$ mice per group. Scale bar = 50 μm. MCD, maternal control diet. MHFD, maternal high-fat diet. All data are displayed as means ± SDs. $^{**}p < 0.01$, $^{***}p < 0.001$, $^{****}p < 0.0001$.

(Supplementary Fig. 3B, C, F and G). The number of goblet cells in each crypt was counted in MCD group as indicated by PAS staining and noticed a significant increase in the *Lrrc19*$^{-/-}$-MCD group (Supplementary Fig. 3D and H). Likewise, we probed the MUC2 production and fucosylation between the WT-MCD group and *Lrrc19*$^{-/-}$-MCD group. The number of MUC2 positive cells in each crypt increased significantly in *Lrrc19*$^{-/-}$-MCD group (Supplementary Fig. 3E and I). In correspondence, an increased number of MUC2^{+}UEA-I^{+} goblet cells in the colonic mucosa of the *Lrrc19*$^{-/-}$-MCD group, as well as an increased expression of *Muc2* in mRNA levels was detected (Supplementary Fig. 3J, K and L). Taken together, the ameliorative effect of LRRC19 depletion on intestinal development, goblet cell differentiation, and MUC2 production and fucosylation was more remarkable in MHFD-fed condition than in the MCD background. We therefore deduce that LRRC19 depletion plays a more pronounced protective role in MHFD condition.

LRRC19 depletion partly reversed the MHFD-induced gut microbiota alteration of offspring

In order to explore the role of the gut microbiota in MHFD-induced intestinal mucus barrier disruption of offspring, fecal metagenomic sequencing of 3 weeks old pups was implemented. No differences were observed in the Shannon and Simpson diversity index of microbiota among offspring in MCD, MHFD, WT-MHFD, and *Lrrc19*$^{-/-}$-MHFD groups at the species level (Fig. 5A). Gut microbiota compositional discrimination was detected by principal coordinate analysis (PCoA) on unweighted UniFrac distances (Fig. 5B). Significant co-clustering of samples by maternal diets

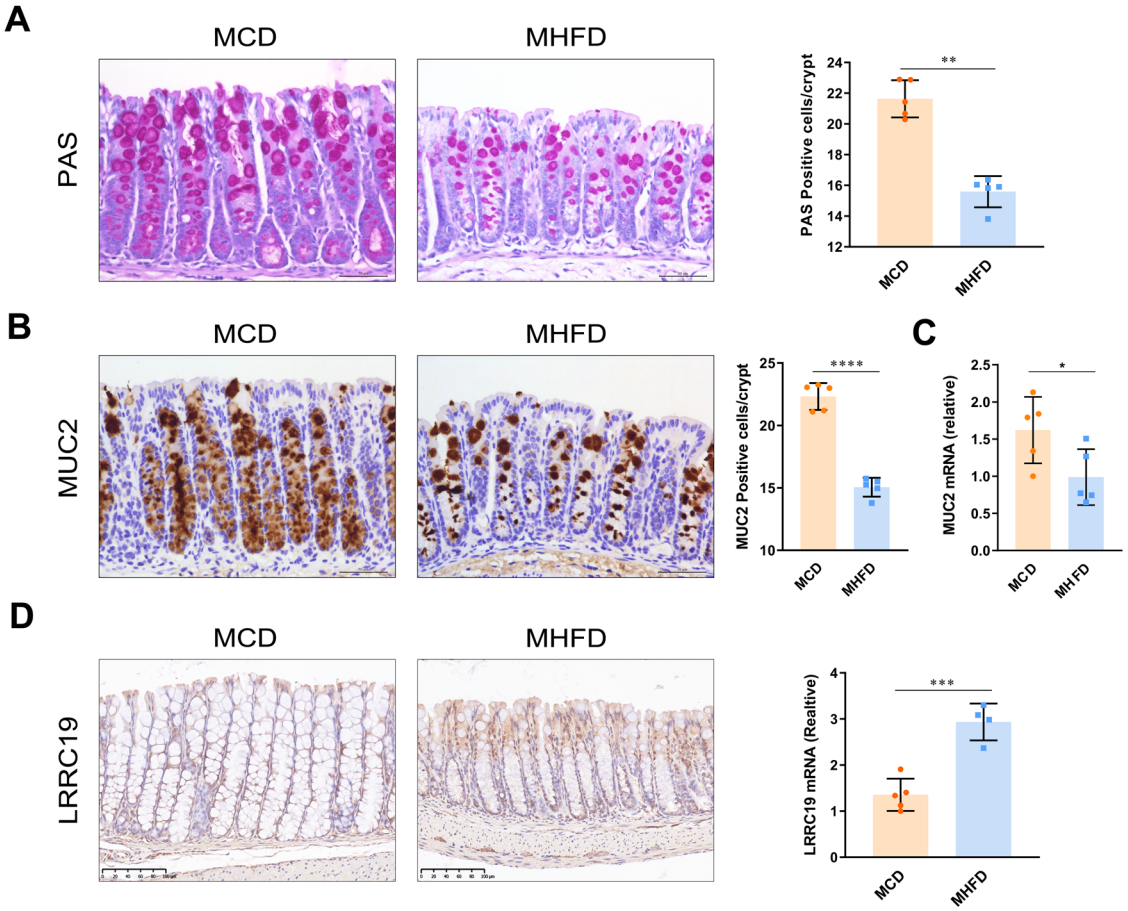

Fig. 2 | Maternal high-fat diet disrupts intestinal barrier and upregulates LRRC19 expression in offspring. A Goblet cells in the colon were assessed by PAS staining between MCD, MHFD groups. Scale bar = 50 μm. **B** The production of MUC2 in the colon was assessed by immunostaining. Scale bar = 50 μm. In (**A**, **B**), the number of positively stained cells in each crypt/villus of five random fields from ×200 images was counted. $n = 5$ mice per group. **C** The relative expression of *Muc2* in mRNA levels was assessed by Realtime-PCR. $n = 5$ per group. **D** The relative expression of LRRC19 was assessed in mRNA levels and by immunostaining. $n = 4$–5 mice per group. Scale bar = 100 μm. MCD, maternal control diet. MHFD, maternal high-fat diet. All data are displayed as means ± SDs. $^{*}p < 0.05$, $^{**}p < 0.01$, $^{***}p < 0.001$, $^{****}p < 0.0001$.

was observed, indicating that MHFD leads to prominent effects on microbiota composition of pups. In agreement, Anosim analysis suggested that the differences between the MCD group and these MHFD-groups were significant (Fig. 5C). In Fig. 5C, "between" represents the differences between different groups, while the box plots of MCD, MHFD, WT-MHFD, and *Lrrc19*$^{-/-}$-MHFD represent the differences within groups. R > 0 indicated that the differences between groups are greater than the differences within groups, and the grouping is reasonable. Meanwhile, the microbiota community structures of each mouse in MCD, MHFD, WT-MHFD, and *Lrrc19*$^{-/-}$-MHFD groups were analyzed (Fig. 5D–F). The microbial composition at the phylum level of each mouse was shown, and notably, a significantly increased ratio of the *Firmicutes*/*Bacteroidetes* was observed in the MHFD group. Meanwhile, *Verrucomicrobia* was decreased in the MHFD group and recovered in the *Lrrc19*$^{-/-}$-MHFD group. Compared with the WT-MHFD offspring, *Proteobacteria* was decreased in the *Lrrc19*-deficient offspring (Supplementary Fig. 4A). Importantly, the relative abundance of *Lactobacillus reuteri* (*L. reuteri*), a beneficial bacterium, was significantly enriched in the *Lrrc19*-deficient offspring, with the highest LDA score computed by LEfSe difference analysis at the species level (Fig. 5E). These, taken together, suggest that LRRC19 depletion could partly reverse the gut microbiota alteration of offspring induced by MHFD.

To determine the potential functions of gut microbiota, the correlation between gut microbiota and microbial metabolism was predicted by microbiota functional analysis. The microbial metabolism discrimination among pups was analyzed by PCoA on unweighted UniFrac distances, and a significant co-clustering of samples by maternal diets was observed (Fig. 6A). Moreover, the relative abundance of orthologs annotated to the KEGG categories at level2 in each sample indicated that amino acid metabolism was a key pathway altered in MHFD pups compared with MCD pups, and this change was also observed between WT-MHFD and *Lrrc19*$^{-/-}$-MHFD groups (Fig. 6B). Correlation analysis of differential species with KEGG metabolic pathways showed a positive correlation between tryptophan metabolism and *L. reuteri*, which has gained the highest LDA score in the *Lrrc19*-deficient offspring (Fig. 6C). Subsequently, the relative abundance of tryptophan metabolism among four groups was analyzed, and notably, an increase in tryptophan metabolism was observed in the *Lrrc19*$^{-/-}$-MHFD group (Fig. 6D). These data indicate that microbial tryptophan metabolism may be involved in the process of LRRC19 depletion alleviating the MHFD-induced intestinal mucus barrier disruption, and LRRC19 may involve in regulating the gut microbiota and microbial metabolism.

LRRC19 depletion promoted the restoration of tryptophan metabolic function in offspring induced by MHFD

Various studies have suggested that the microbiota-associated tryptophan metabolites, such as indole-3-ethanol, indole-3-pyruvate, and indole-3-acetaldehyde, could enhance the intestinal mucosal barrier function[27]. Since the change of tryptophan metabolism was observed by the microbiota functional prediction analysis, we next detected and analyzed the microbiota-derived tryptophan metabolites by metabolomic sequencing and focused on the function of tryptophan metabolism in the protection of

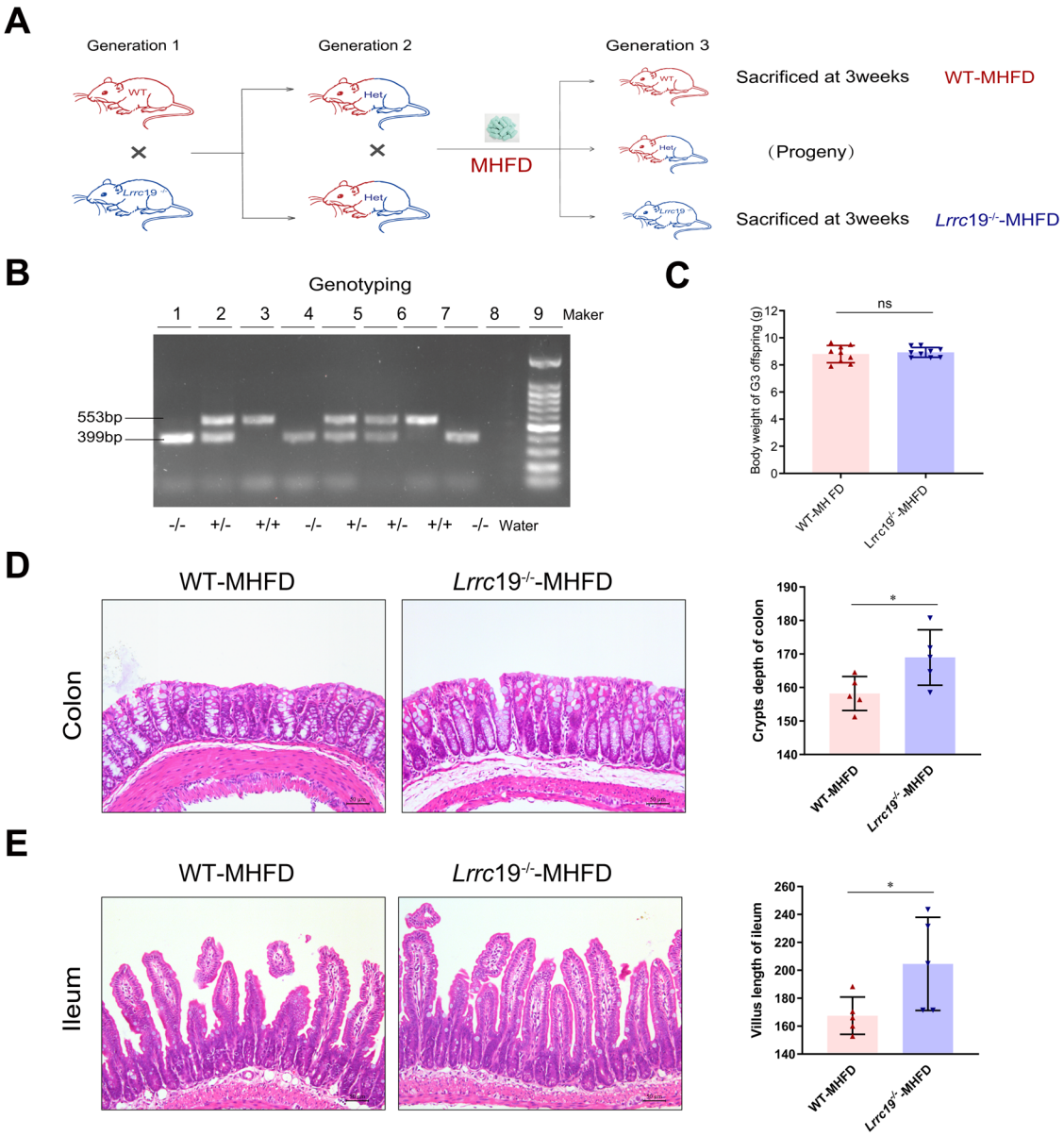

Fig. 3 | Maternal high-fat diet disrupts offspring intestinal development via LRRC19. A Experimental flow diagram of WT-MHFD and *Lrrc19*$^{-/-}$-MHFD groups. *Lrrc19*$^{+/-}$ mice derived from the *Lrrc19*$^{+/+}$ and *Lrrc19*$^{-/-}$ parents were crossbred to generate different genotypes of offspring, and the *Lrrc19*$^{+/+}$ and *Lrrc19*$^{-/-}$ pups were selected for further analysis at 3 weeks old. The heterozygous *Lrrc19*$^{+/-}$ female mice were fed a high-fat diet during the period of gestation and lactation as described. **B** Genotype identification in the offspring of heterozygous mice. PCR of total DNA extracted from tail. +/+, wild-type mouse. +/–, heterozygous mouse. –/–, *Lrrc19* knockout mouse. **C** Body weight of pups at 3 weeks of age in WT-MHFD and *Lrrc19*$^{-/-}$-MHFD groups. $n = 9$ per group. **D** H&E staining of colonic tissues and colon crypts depth in the 3 weeks old offspring between WT-MHFD and *Lrrc19*$^{-/-}$-MHFD groups. Five random fields from ×200 images were viewed for each mouse and the depth of well-orientated crypts was measured. Scale bar = 50 μm. $n = 5$ mice per group. **E** H&E staining of small intestinal tissues and the villus length of ileum in the 3-week-old offspring in WT-MHFD and *Lrrc19*$^{-/-}$-MHFD groups. Five random fields from ×200 images were viewed for each mouse and the length of well-orientated villi was measured. $n = 5$ mice per group. MHFD, maternal high-fat diet. WT, wild type (*Lrrc19*$^{+/+}$). Het, heterozygous type (*Lrrc19*$^{+/-}$). ns, not significant. All data are displayed as means ± SDs. $^{*}p < 0.05$.

intestinal mucus barrier during MHFD. Among microbiota-derivate tryptophan metabolites, a relatively decreased abundance of indoles in the MHFD group versus to MCD group was observed, and this change was restored to some extent in the LRRC19 depletion offspring (Fig. 7A, B and C). Furthermore, the levels of several indole derivatives were assessed. Based on the accurate quantification measurements of tryptophan metabolites shown in the volcano plot and vioplot (Fig. 8D, E), a decreased level of three kinds of indole derivatives in the MHFD offspring compared with MCD was specifically identified, such as the level of indole-3-acetic acid (IAA), producing by the gut microbiota from tryptophan. Consistently, IAA gained the highest Z-score in the MCD group (Supplementary Fig. 4B). Additionally, an increased level of IAA was observed in the *Lrrc19*-deficient offspring compared with WT-MHFD offspring.

In order to identify the potential implicated bacteria with tryptophan metabolites, we performed a correlation analysis at the species levels. Interestingly, a negative correlation between IAA and *Escherichia coli* as well as a positive correlation between IAA and *Bifidobacterium pseudolongum* were observed (Supplementary Fig. 4C). Moreover, we observed that *Bacteroidales_bacterium_M10*, *Bacteroidales_bacterium_M1* and *Bacteroidales_bacterium_M12* were positively correlated with IAA, while *Bacteroidales_bacterium_M6* were negatively correlated with IAA. Thus, these data further infer the involvement of the gut microbiota in

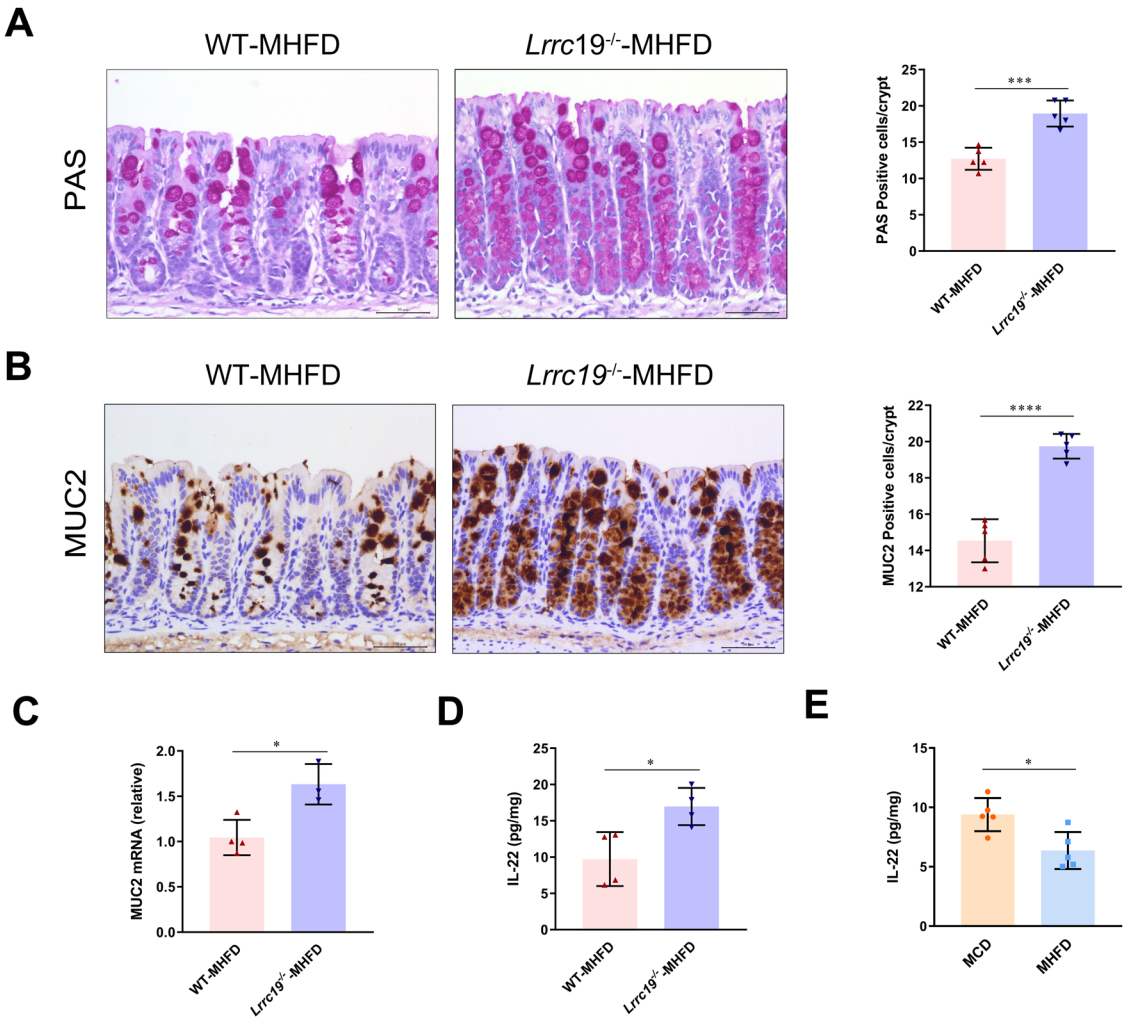

Fig. 4 | LRRC19 mediates disruption on intestinal barrier in maternal high-fat diet offspring. A Goblet cells in the colon were assessed by PAS staining and the PAS positive cells of each crypt were counted between WT-MHFD and *Lrrc19*$^{-/-}$-MHFD groups. The number of positively stained cell in each crypt of five random fields from ×200 images were counted. Scale bar = 50 μm. $n = 5$ mice per group. **B** The production of MUC2 in the colon was assessed by immunostaining and the MUC2 positive cells of each crypt were counted in WT-MHFD and *Lrrc19*$^{-/-}$-MHFD groups. The number of positively stained cell in each crypt of five random fields from ×200 images were counted. Scale bar = 50 μm. $n = 5$ mice per group. **C** The relative expression of MUC2 in mRNA levels was assessed by Realtime-PCR in WT-MHFD and *Lrrc19*$^{-/-}$-MHFD groups. $n = 3$–4 mice per group. **D** IL-22 levels in the colon were detected by ELISA in WT-MHFD and *Lrrc19*$^{-/-}$-MHFD groups. $n = 4$ per group. **E** IL-22 levels in the colon were detected by ELISA in in MCD and MHFD groups. $n = 5$ per group. MCD, maternal control diet. MHFD, maternal high-fat diet. WT, wild type (*Lrrc19*$^{+/+}$). All data are displayed as means ± SDs. $^{*}p < 0.05$, $^{***}p < 0.001$, $^{****}p < 0.0001$.

contributing to MHFD-induced tryptophan metabolism disorder and indicate that depletion of LRRC19 may shape the gut microbiota to promote the restoration of tryptophan metabolic function in offspring.

IAA promoted IL-22 transcription in AhR-dependent ILC cells and facilitated MUC2 fucosylation

Tryptophan metabolites generally influence the gut barrier function by activating IL-22 production as reported[28], among which, IAA, a ligand of the AhR, may play a key role. Meanwhile, IL-22 is acknowledged to then involve in the regulation of goblet cells differentiation and mucins expression[29]. To further investigate the underlying barrier-protective mechanisms of IAA in regulating MUC2 fucosylation, we detected the levels of IL-22, IL-22 producing-innate lymphocytes and mucus barrier MUC2 expression among WT-Control, WT-IAA, *Ahr*$^{-/-}$-Control and *Ahr*$^{-/-}$-IAA groups (Fig. 8A). Flow cytometry analysis showed an increase in IL-22-producing ILC3s in WT-IAA group compared to WT-Control group, while depletion of AhR relatively reduced ILC3s. AhR deficiency could largely reverse the promoting effects of the supplemental IAA as no significant changes of IL-22-producing ILC3s proportion were observed in *Ahr*$^{-/-}$-IAA group comparing with *Ahr*$^{-/-}$-Control group (Fig. 8B and C). An increased production of colonic cytokine IL-22 was observed in WT-IAA group compared with WT-Control group, while IAA supplement brought no elevated expression of IL-22 in the AhR-deficient offspring (Fig. 8D). We then investigated the mucus barrier function by immunohistochemistry and immunostaining. The number of MUC2 positive cells in each crypt was significantly increased in WT-IAA group compared with WT-Control group, while compared with *Ahr*$^{-/-}$-Control group, the number of MUC2 positive cells in each crypt in *Ahr*$^{-/-}$-IAA group did not increase after IAA treatment (Fig. 8E and G). Moreover, the number of MUC2^{+}UEA-I^{+} goblet cells in the colon mucosa of WT-IAA group was significantly increased compared with WT-Control group, indicating an increase of mucin fucosylation. Meanwhile, we found no difference between the *Ahr*$^{-/-}$-Control group and *Ahr*$^{-/-}$-IAA group, which indeed confirmed that IAA depended on AhR to promote differentiation of goblet cells and expression of MUC2 fucosylation (Fig. 8F and H). These data, taken together, indicate that supplemental IAA restores the mucus barrier function by expanding IL-22-producing ILC3s and facilitating MUC2 fucosylation, and this promoting effect is dependent on AhR. Hence, our data suggest that IAA supplementation may play a protective role in regulating intestinal mucus barrier through the tryptophan metabolite-AhR-IL-22 axis.

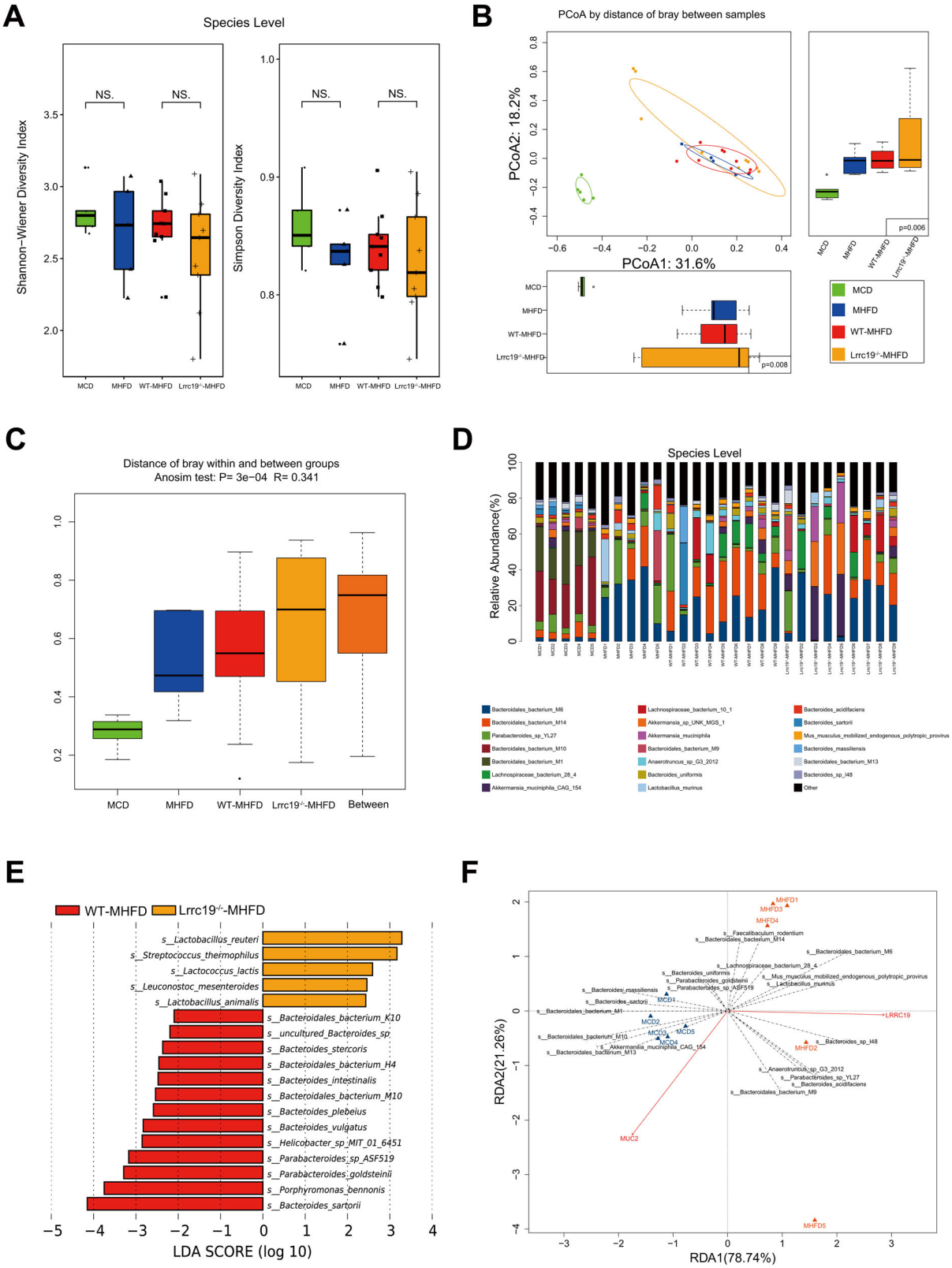

Fig. 5 | LRRC19 depletion partly reverses the altered gut microbiota in maternal high-fat diet offspring. A, **B** Total fecal bacteria from 3 weeks old offspring mice among MCD, MHFD, WT-MHFD and *Lrrc19*$^{-/-}$-MHFD groups were detected by metagenomic sequencing, Shannon and Simpson diversity index at species level were shown (**A**), and beta diversity was measured by the unweighted Unifrac principal coordinate analysis (PCoA) (**B**). **C** Anosim analysis of species was used to determine whether the differences between groups are significantly greater than the differences within groups. **D** Relative abundance of bacterial taxa at the species level among four groups. **E** Linear discrimination analysis (LDA) Effect Size (LEfSe) difference analysis at species level between WT-MHFD and *Lrrc19*$^{-/-}$-MHFD groups were shown. **F** The relationship between gut microbiota and *Muc2* expression as well as *Lrrc19* expression was reflected by redundancy analysis. MCD, maternal control diet. MHFD, maternal high-fat diet. WT, wild type (*Lrrc19*$^{+/+}$). In MCD and MHFD groups, $n = 5$; In WT-MHFD and *Lrrc19*$^{-/-}$-MHFD groups, $n = 9$. Bars indicated means ± SDs.

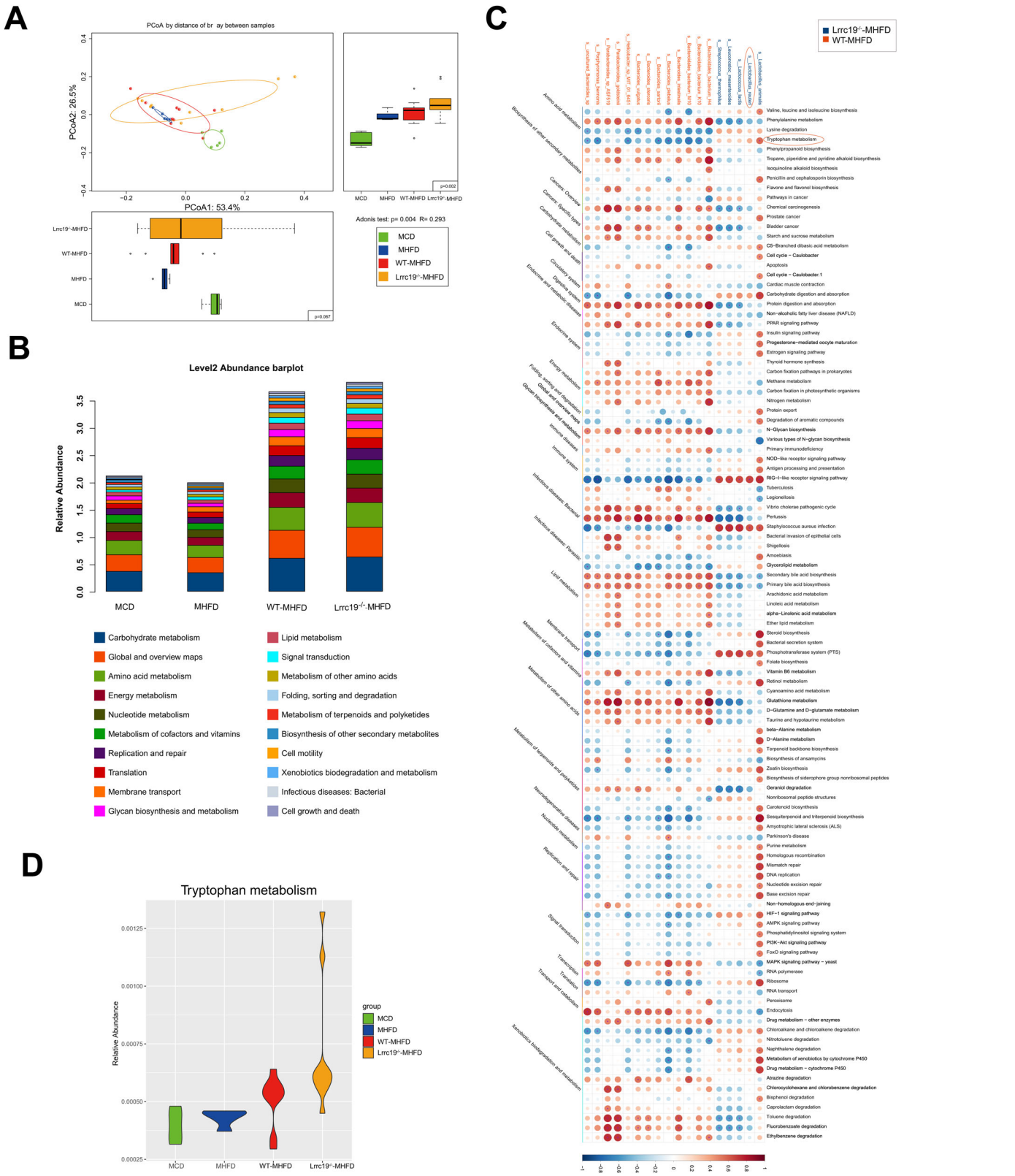

Fig. 6 | LRRC19 may engage in the regulation of gut microbiota and tryptophan metabolism. A Metabolic function among four groups was measured by the unweighted Unifrac principal coordinate analysis (PCoA). **B** The relative abundance of orthologs annotated to the KEGG categories at level2 among four groups. **C** Corrplot of differential species and metabolic pathways between WT-MHFD and *Lrrc19*$^{-/-}$-MHFD groups. **D** Relative abundance of tryptophan metabolism among four groups. MCD, maternal control diet. MHFD, maternal high-fat diet. WT, wild type (*Lrrc19*$^{+/+}$). In MCD and MHFD groups, $n = 5$; In WT-MHFD and *Lrrc19*$^{-/-}$-MHFD groups, $n = 9$. Bars indicated means ± SDs.

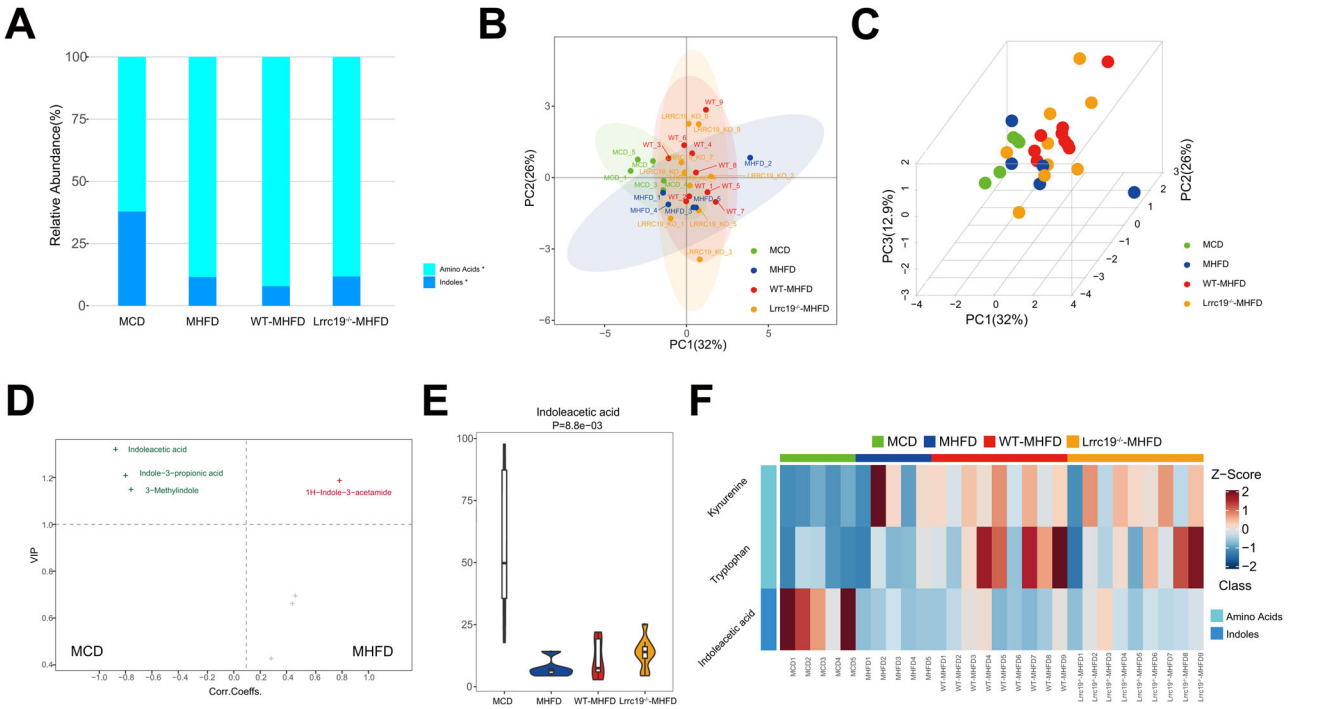

Fig. 7 | LRRC19 may promote the restoration of tryptophan metabolic function in maternal high-fat diet offspring via shaping the gut microbiota. A Relative abundance of indoles and amino acids producing by microbiota in the individual fecal samples among four groups. **B**, **C** Principal component scores were respectively shown as 2D plot (**B**) and 3D plot (**C**) (determined by unweighted UniFrac analysis). **D** Reliable metabolic markers were screened by volcano plot. Volcano plot comprehensively inspected the contribution of metabolites to the model group (Variable importance in the projection, VIP) and reliability of metabolites (the Correlation Coefficients, Corr. Coeffs). Metabolites that significantly increase in the MCD group are shown in green, while those significantly increase in the MHFD group are shown in red. **E** Levels of IAA among four groups were shown in the violplot. **F** Z-Score of differential metabolites was shown as point plot and heatmap. MCD, maternal control diet. MHFD, maternal high-fat diet. WT, wild type (*Lrrc19*$^{+/+}$). In MCD and MHFD groups, $n = 5$; In WT-MHFD and *Lrrc19*$^{-/-}$-MHFD groups, $n = 9$. Bars indicated means ± SDs.

Discussion

As one of the potential risk factors, MHFD has been reported to affect the early colonization of gut microbiota which could further influence the establishment of the immune system as well as disrupt the intestinal mucosal barrier in multiple studies[5,30]. However, to date, few studies have investigated the mechanisms of the adverse effect of MHFD on offspring. LRRC19 has been known as a novel intestinal epithelial pattern recognition receptor, involved in the recognition of gut microbiota, the activation of immune pathways, and the regulation of gut epithelial barrier function[17,24]. In this study, we investigated the role of LRRC19 in the alteration of gut microbiota and disruption of intestinal mucus barrier induced by MHFD. Our results demonstrated that LRRC19 depletion could improve the MHFD-induced gut microbiota alteration, and alleviate intestinal mucus barrier disruption of offspring exposed to MHFD by increasing IAA level and promoting the secretion and fucosylation of MUC2 (Fig. 9). These results may at least partially explain how a MHFD induces gut microbiota alteration and intestinal mucus barrier disruption thus leading to the susceptibility to disease in adulthood of offspring.

The intestinal mucosal barrier is composed of epithelial cells and overlying mucus layers secreted by goblet cells. The mucus layer is mainly composed of mucins, of which MUC2 is the most abundant secretory mucin[18,31]. Previous studies have indicated that fucosylated or O-glycosylated mucins are involved in the modulation of gut microbiota, and the microbiota composition is an important factor in regulating intestinal mucus barrier function, which is crucial for maintaining gut health[32,33]. Moreover, studies have shown that multiple genetic and environmental factors shape the gut microbiota and alter the integrity of the mucus layer directly or indirectly[31,34,35]. In this study, we confirmed that MHFD reduced the secretion and fucosylation of MUC2 and thus impaired the intestinal mucus barrier function, as previous studies reported[11,36,37]. Considering the lacking comprehension between MHFD and the disruption of the intestinal mucus barrier, we focus on the relationship between intestinal epithelial receptors and gut microbiota. Intestinal epithelial receptors involve in maintaining the host immune homeostasis by regulating the recognition of gut microbiota[19]. A HFD during the perinatal period could alter the gut microbiota, fetal gut barrier proteins, and immune markers as reported in a recent study, thereby impairing intestinal barrier integrity and being implicated in fetal gut inflammation[37]. Our previous study has reported that LRRC19 can recognize gut microbiota and activate NF-κB and MAPK pathways to induce the production of proinflammatory cytokines, chemokines and antimicrobial substances, promoting inflammatory responses, while *Lrrc19* deficiency reduces gut inflammatory responses[17]. In addition, our recent study has indicated that LRRC19 can promote intestinal epithelial permeability through reducing the expression of ZO-1, ZO-3, and occludin. Moreover, tighter junctions and narrower gaps between colonic cells were observed by transmission electron micrographs in *Lrrc19*$^{-/-}$ mice[24]. All of these implied that LRRC19 is involved in intestinal inflammation and impairment of gut barrier function. Interestingly, our present study found that MHFD up-regulated the expression of LRRC19, whereas LRRC19 depletion improved the production and function of MUC2, indicating alleviation of intestinal mucus barrier disruption in MHFD offspring. The data we present here clearly showed that LRRC19 can be involved in the MHFD-induced impaired intestinal mucus barrier of offspring.

To investigate the potential mechanisms whereby LRRC19 depletion might impact the microbiota to protect the MHFD-induced intestinal mucus barrier disruption, we further analyzed the intestinal microbiota and microbial metabolism. On the whole, our results highlight the coordination of microbiota alteration along with associated metabolic pathway and intestinal mucus barrier disruption of offspring exposed to MHFD. Previous

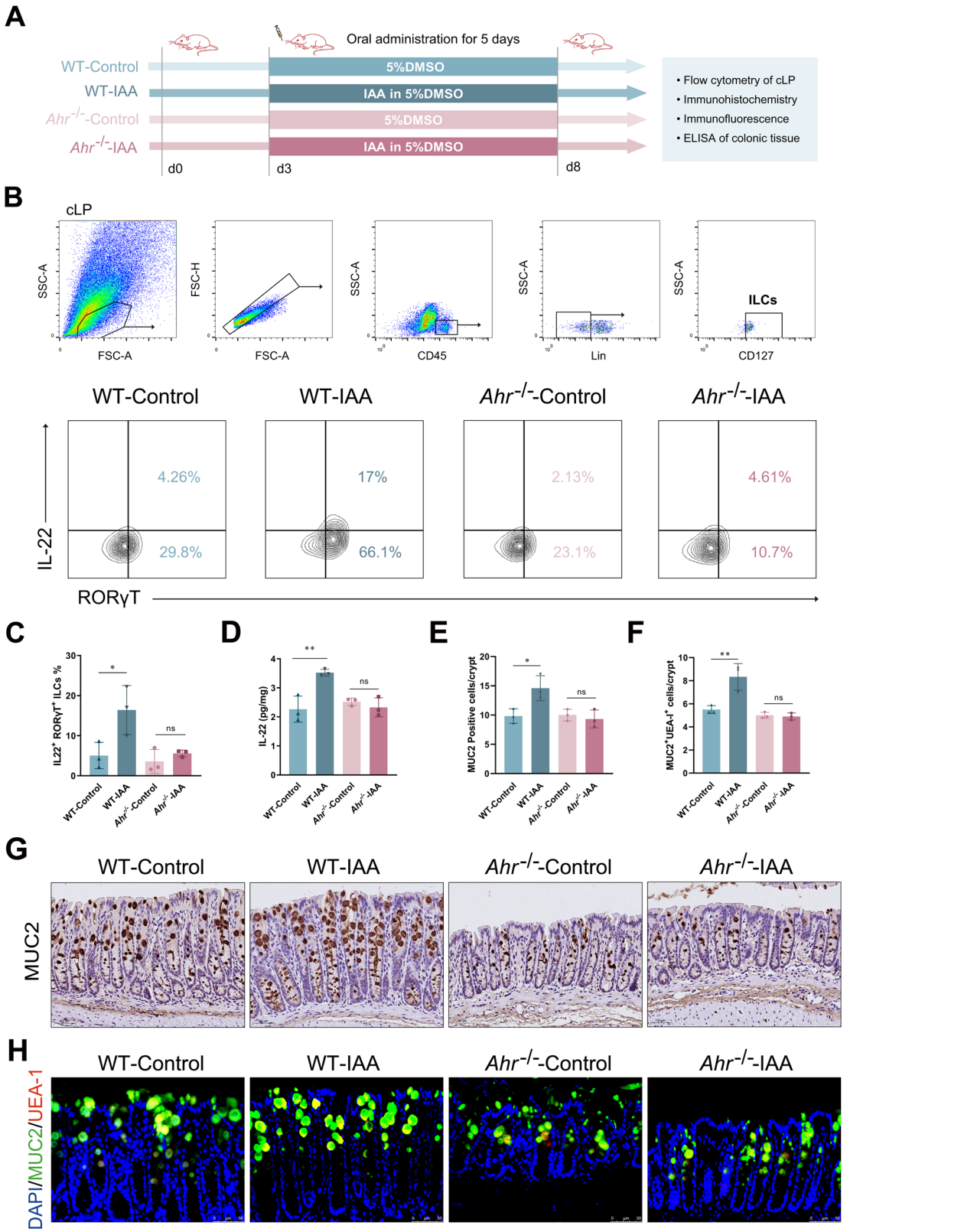

Fig. 8 | IAA ameliorates intestinal barrier function via AhR-ILC3-IL-22-MUC2 axis. A Experimental flow chart. **B**, **C** Colonic lamina propria lymphocytes were collected and the percentages of IL22^{+}RORγT^{+} ILC3 in colonic lamina propria lymphocytes were analyzed by flow cytometry (**B**), and the quantification was shown (**C**). (D) IL-22 levels in the colon were detected by ELISA in WT-Control group, WT-IAA group, *Ahr*$^{-/-}$-Control group and *Ahr*$^{-/-}$-IAA group. $n = 3$–5 mice per group. **E**, **G** The production of MUC2 in the colon was assessed by immunostaining (**G**), and the numbers of MUC2 positive cells in each crypt were counted (**E**). Scale bar = 50μm. $n = 5$ mice per group. **F**, **H** Representative epifluorescence staining for goblet cells in the colon using an antibody against MUC2 (green) and the lectin UEA-I (red) with DAPI (blue) as the counter stain (**H**). Quantitative analysis of both MUC2 and UEA-I-positive (MUC2^{+}UEA-I^{+}) goblet cell number of per crypt in WT-Control group, WT-IAA group, *Ahr*$^{-/-}$-Control group and *Ahr*$^{-/-}$-IAA group was counted (**F**). $n = 3$–5 mice per group. IAA, indoleacetic acid; MUC2, Mucin-2; WT, wild type (*Ahr*$^{+/+}$); ns, not significant. All data are displayed as means ± SDs. $^{*}p < 0.05$, $^{**}p < 0.01$, $^{****}p < 0.0001$.

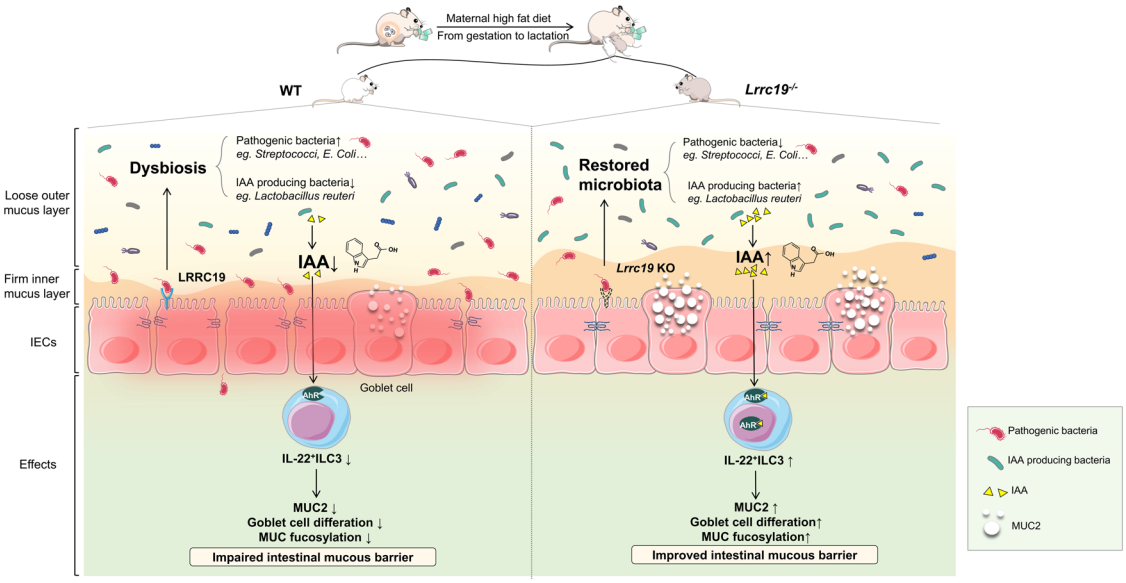

Fig. 9 | LRRC19 depletion alleviates intestinal mucus barrier disruption of offspring exposed to maternal high-fat diet. Maternal high-fat diet alters gut microbiota, resulting in a higher relative abundance of pathogenic bacteria, which could penetrate the intestinal mucus layer and be recognized by LRRC19. The activation of LRRC19 further aggravates the alteration of gut microbiota. Subsequently, the decreased abundance of IAA-producing bacteria (such as Lactobacillus_reuteri) results in a decreased level of IAA, thus reducing the secretion and fucosylation of MUC2 as well as differentiation of goblet cells. Ultimately, the gut epithelial mucus barrier function is compromised. In contrast, LRRC19 depletion partly reverses the alteration of gut microbiota and promotes the restoration of tryptophan metabolic function, and alleviates the intestinal mucus barrier disruption of offspring exposed to MHFD. IAA improved the mucus barrier function by increasing the number of IL-22$^+$ ILC3 cells in an AhR-dependent manner. MHFD, maternal high-fat diet. LRRC19, leucine-rich repeat C19. WT, wild type (*Lrrc19*$^{+/+}$). *Lrrc19* KO, *Lrrc19* knockout (Lrrc19$^{-/-}$). IAA, indoleacetic acid.

studies have indicated that MHFD could alter the microbiota of early-stage offspring[8,11,38]. In this study, the composition and diversity of microbiota in MHFD offspring presented significant alterations consistently, with the characteristic of a significantly increased ratio of the Firmicutes/Bacteroidetes. We have previously found that under normal conditions, LRRC19 is highly expressed in the intestinal epithelium and is involved in regulating the development of the intestinal immune system. The intestinal microbiota can activate LRRC19, which mediates the expression of regenerating islet-derived (REG) proteins through the TNF receptor-associated factor 2 (TRAF2) and TRAF6-mediated NF-κB signaling pathway. Members of the REGs can kill Gram-positive bacteria in the intestine. After LRRC19 knockdown, activation of the NF-κB signaling pathway is reduced and expression of REGs is decreased, which leads to altered bacterial structure. In our study, we also found changes in the structure of the microbiota[17]. Specifically, knocking out *Lrrc19* markedly increased the proportions of *Bacteroidetes*, which harbor abundant tryptophanases and have the ability to transform tryptophan into several molecules[39]. Moreover, some *Muc2*-associated bacteria, such as *Akkermansia_muciniphila_CAG_154*, were decreased in the MHFD group. Multiple studies have indicated that *Akkermansia muciniphila* can encode the mucin-dependent enzymes and balance the mucin degradation and reservation in maintaining intestinal mucosal barrier function. In addition, *Akkermansia muciniphila* would restore the expression of gut epithelial tight junction proteins occludin to enhance the intestinal barrier function[40]. Interestingly, a slight increase of *Akkermansia_muciniphila_CAG_154* in the *Lrrc19*-deficient offspring was observed in this study. Hence, our present data suggested that MHFD may disrupt the intestinal mucus barrier by inducing the alterations of mucin-associated microbiota, and LRRC19 is involved in this process. On the other hand, in view of the significant increase of *Lrrc19*-associated bacteria in the MHFD group, such *Bacteroidales_bacterium_M6* as shown in our study, we hypothesized that MHFD may induce the increase of some *Lrrc19*-associated bacteria, thus up-regulating the expression of LRRC19. Although our study verified that LRRC19 is involved in the process of MHFD-induced gut microbiota alteration and intestinal mucus barrier disruption, the relationship between MHFD and LRRC19, as well as the interaction between LRRC19 and gut microbiota remains to be further explored.

As messengers of microbiota and host, metabolites produced by gut microbiota play a critical role in maintaining intestinal immune homeostasis and gut barrier integrity[23]. Previous studies have shown that dietary alteration could affect gut microbiota composition and thus influence bacterial metabolism[41–43]. For instance, HFD induced gut dysbiosis and decreased the production of short-chain fatty acids and tryptophan metabolites[44,45]. Similarly, alterations of metabolites, such as short-chain fatty acids and tryptophan metabolites, had been observed in inflammatory bowel disease patients[46]. In our study, pups with MHFD showed a lower capacity of tryptophan metabolism, while the decreased level of tryptophan metabolism was restored in *Lrrc19*$^{-/-}$-MHFD offspring, which revealed that perturbations were transmitted to offspring despite no direct HFD exposure.

Furthermore, we analyzed the intestinal microbial tryptophan metabolites to investigate whether the potential protective role of LRRC19 depletion is mediated by tryptophan metabolism. Particularly, microbial tryptophan metabolites can increase gut barrier function and maintain intestinal immune homeostasis via the AhR as reported[27,47–49]. In the present study, we observed that *Lrrc19*-deficient offspring notably increased the level of tryptophan metabolite IAA when exposed to MHFD. Moreover, the relative abundance of *L. reuteri* was significantly enriched in the *Lrrc19*-deficient offspring. *L. reuteri* is one of the most extensively researched probiotic species and has been widely employed as a probiotic for numerous years[50]. The latest literature shows that *L. reuteri* reverses the impaired microbial tryptophan metabolism in colitis mice by enhancing the expression of metabolizing enzymes leading to increased indole-3-propionic acid and IAA syntheses[51]. This suggests that IAA may be a potentially beneficial metabolite involved in mucosal barrier improvement in *Lrrc9*-deficient mice exposed to MHFD. Previous studies have suggested that tryptophan metabolites can significantly activate AhR and then increase the expression of downstream cytokines like IL-22, thus playing a key role in gut homeostasis[47,52] and strengthening the integrity of the intestinal mucus layer[53,54] by increasing the number of goblet cells, and directly induce the

expression of mucin genes, as well as promote fucosylation and glycosylation of MUC2[33,55,56]. To investigate the mechanisms of tryptophan metabolites in regulating the intestinal mucus barrier function, we focused on the typical metabolite IAA and detected the levels of colonic cytokine IL-22 and IL-22-producing lymphoid cell ILC3, we found that a noticeable increased production of IL-22 as well as ILC3 in WT-IAA group compared with WT-Control group without IAA supplementation, while this activation was largely reversed by AhR deficiency. Similar results were observed in MUC2 immunohistochemistry and immunofluorescence staining of $MUC2^{+}$ goblet cells of the colon. These results taken together indicated that tryptophan metabolites promote IL-22 transcription through AhR-dependent ILC3s, and eventually facilitate MUC2 fucosylation. Our findings in brief supported that LRRC19 can indirectly regulate the process of tryptophan metabolism, and subsequently affect the intestinal mucus barrier function via tryptophan metabolite-AhR-IL-22 axis.

In particular, we performed a correlation analysis between indole derivatives and bacteria. Studies have indicated that *Bifidobacteria* can protect against microbiota-mediated colonic mucus deterioration[35,57]. In this study, we found that the abundance of *Bifidobacterium pseudolongum*, which showed a positive correlation with IAA, was decreased in MHFD groups while partly reversed in the *Lrrc19*-deficient offspring. And notably, we found the relative abundance of *Lactobacillus* genus, including *L. reuteri*, was restored in *Lrrc19*-deficient offspring as compared with WT offspring. Our previous study has shown that LRRC19, as a potential bacterium recognition receptor, is involved in the recognition of *Lactobacillus*[17]. Recently, studies have shown that MHFD induced social deficits and a change of gut microbiota in offspring mice, particularly, a reduction of the commensal bacterial species *L. reuteri* has been observed. More importantly, the bacterial species *L. reuteri* reversed the social deficits in MHFD offspring[58]. As a well-studied probiotic bacterium, *L. reuteri* has been reported to promote gut mucosal integrity[59,60]. Previous studies have reported that *L. reuteri* can produce indole-3-aldehyde, a tryptophan-indole derivative, and induce IL-22 production via activation of AhR to provide mucosal protection[61]. Our present study has supported that *L. reuteri* can increase goblet cell number and mucin fucosylation, thus mediating protection from intestinal mucus barrier disruption. Therefore, MHFD may lead to the tryptophan metabolism disorder by inducing the changes in IAA-associated bacteria.

There are a few limitations of this study. The early-life period is characterized by a remarkable epigenetic plasticity. Epigenetic modification may be an important mechanism involved in the long-term immune adaptations by early-life environmental stimuli. However, this article primarily focuses on discussing the impact of early life nutrition on offspring gut health through the lens of gut microbiome and metabolic dysregulation, without addressing the role of epigenetics. This represents a limitation of this study. In addition, this article has identified the potential beneficial tryptophan bacterial metabolite IAA. However, the improvement effect of IAA on maternal high-fat diet-induced offspring intestinal barrier damage has not been fully evaluated. In the future, more experiments may be needed to explore the regulatory mechanism of IAA on intestinal mucus barrier function.

Conclusions

In conclusion, these data suggested that LRRC19 depletion contributed to the colonization of health-promoting bacteria, such as *L. reuteri*, which enhances the microbiota-mediated tryptophan metabolism and increases the level of IAA. It was hypothesized that IAA can activate AhR and further increase the production of IL-22. Subsequently, IL-22 alleviates the gut mucus barrier disruption of MHFD offspring by promoting the production and fucosylation of MUC2. Thus, our results supported the hypothesis that host factors are involved in the MHFD-induced intestinal mucus barrier disruption in offspring. These present data would provide implications for the mechanisms of MHFD-induced gut dysbiosis and intestinal mucosal barrier disruption of offspring, and may partially explain the increased susceptibility to multiple diseases in adulthood.

Materials and methods

Animals and treatment

All the animal care and experimental procedures were performed according to the guidelines of the Institutional Animal Care and Use Committee at Tianjin Medical University, and the protocols were approved by the Animal Ethical and Welfare Committee of Tianjin Medical University. We have complied with all relevant ethical regulations for animal use. Ten male and 10 female 7-week-old C57BL/6 mice were purchased from the Institute of Laboratory Animal Science, Chinese Academy of Medical Sciences & Peking Union Medical College. Animals were housed in the specific pathogen-free facility and maintained in a light- and temperature-controlled circumstance, and had access to chow and water ad libitum. All mice were acclimatized for 7 days and then mated to produce offspring on a control diet. Ten female mice were confirmed to be pregnant and were randomly assigned to maternal control diet (MCD) group and MHFD group. MCD group was fed with a control diet (H10010; 3.85 kcal/g; 10 E% fat, 20 E% protein, 70 E% carbohydrate), whereas MHFD group was fed with a high-fat diet (H10060; 5.24 kcal/g; 60 E% fat, 20 E% protein, 20 E% carbohydrate) constantly during gestation (3 weeks) and lactation (3 weeks) period. Pregnant mice were group-housed dependent on diet and then placed in separate housing cages one week before delivery. Total 16 pups from 5 litters were delivered vaginally in the MCD group, and 16 pups from 5 litters were delivered vaginally in the MHFD group. The body weights of each pup were recorded when weaning at postnatal week 3 and the stool samples were collected. Subsequently, pups were sacrificed under anesthesia and then the totality of the intestinal segment was removed immediately (Fig. 1A). The samples were formalin fixed and then embedded into paraffin as intestinal and colonic Swiss rolls, or were rapidly dissected and then stored at −80 °C.

Considering the influence of maternal genotype and littermate effects, littermate reared WT mice with the same parental genotype were selected as controls for $Lrrc19^{-/-}$ mice. Thus, $Lrrc19^{+/-}$ heterozygous mice were used as parents, and then wild type (WT, $Lrrc19^{+/+}$) and $Lrrc19^{-/-}$ offspring mice were identified for experiments. *Lrrc19* knockout ($Lrrc19^{-/-}$) male mice were kindly provided by Professor Yang RC from Nankai University, China. WT female mice were paired with $Lrrc19^{-/-}$ male mice to generate the first filial generation (F1). Afterwards, adult heterozygous F1 mice derived from the $Lrrc19^{+/+}$ and $Lrrc19^{-/-}$ parents were crossbred to generate F2 with different genotypes, and the pregnant $Lrrc19^{+/-}$ female mice were kept together and then placed in separate housing cages one week before delivery.

$Lrrc19^{+/-}$ female mice were constantly fed with a high-fat diet throughout gestation and lactation period, while other same-background $Lrrc19^{+/-}$ female mice were fed with MCD. Under these conditions, $Lrrc19^{-/-}$ F2 were cohoused with their littermates ($Lrrc19^{+/+}$ and $Lrrc19^{+/-}$). After weaning at 3 weeks of age, germline transmission of the *Lrrc19* allele was verified by PCR using tail DNA of F2 (Fig. 3B). There were three different genotypes ($Lrrc19^{+/+}$, $Lrrc19^{+/-}$, and $Lrrc19^{-/-}$). 9 $Lrrc19^{+/+}$ pups (WT-MHFD group), 9 $Lrrc19^{-/-}$ pups ($Lrrc19^{-/-}$-MHFD group), as well as 5 $Lrrc19^{+/+}$ pups (WT-MCD group) and 5 $Lrrc19^{-/-}$ pups ($Lrrc19^{-/-}$-MCD group) were used for further studies. To avoid the same cage effect, we randomly selected one mouse per litter for tissue pathology and molecular biology experiments. The body weights of the selected pups were recorded when weaning and the stool samples were collected, then, pups were sacrificed according to the procedure (Fig. 3A and Supplementary Fig. 3A). Although both of mice from the MHFD group and the WT-MHFD group have the same genotype with $Lrrc19^{+/+}$, they belong to different cohorts. The parents of the mice in the MHFD group were WT. The parents of the mice in WT-MHFD group were LRRC19 heterozygous mice bred from WT mice and $Lrrc19^{-/-}$ mice.

7-week-old male AhR knockout ($Ahr^{-/-}$) mice and 7-week-old male wild type (WT, $Ahr^{+/+}$) mice were kindly provided by Professor Yang RC from Nankai University, China. To explore how IAA regulates intestinal mucus layer through AhR, the WT mice and $Ahr^{-/-}$ were divided into four groups: WT-Control group, WT-IAA group, $Ahr^{-/-}$-Control group and $Ahr^{-/-}$-IAA group. Drug administration (500 mg/kg IAA dissolved in 5% DMSO or vehicle 5% DMSO) was performed daily by oral gavage (Fig. 8A).

All mice were gavaged constantly for 5 days and were sacrificed on the 6th day. The colon tissues were formalin fixed and then embedded into paraffin as colonic Swiss rolls, or were rapidly processed to isolate colonic lamina propria cells.

Ethics statement

All experiments involving animals were conducted according to the ethical policies and procedures approved by the Institutional Animal Care and Use Committee of Tianjin Medical University, Tianjin, China (Approval no. TMUaMEC 2021017).

DNA fingerprint analysis for genotyping

Genomic DNA was isolated from the tails of offspring using TIANcombi DNA Lyse&Det PCR Kit (TIANGEN, Inc., China) to identify the genotype. DNA was used as a template for PCR amplification of the targeted *Lrrc19* allele. The PCR conditions: 95 °C 10 min, 95 °C 30 s (32x), 58 °C 30 s, 72 °C 1 min. The specific primers used for genotype identification of mice were as follows: *Lrrc19*-GF3, AGTCTGTAGTTTCCCGAACACTGC; *Lrrc19*-GR3, TGGTGTTGTTGCCACTGTACTGC and Neo5R, GGCTGGACGTAAACTCCTC[26]. Products were visualized with 1.0% (wt/vol) agarose gel. The single stripe shown on 553 bp indicated a genotype of $Lrrc19^{+/+}$, and the single stripe shown on 399 bp indicated a genotype of $Lrrc19^{-/-}$.

Histology and immunohistochemistry

Formalin-fixed paraffin slices (4-μm) were used for haematoxylin and eosin staining after deparaffinization and hydration. At least five random fields from ×200 images were viewed under light microscopy (Leika DM5000 B, Germany) for each mouse. The intestinal development was assessed by measuring the well-orientated villi length of intestine and the well-orientated crypts depth of colon. The length from crypt opening to the tip of the villi was measured as villi length, and the length from the crypt base to its opening was measured as crypt depth[62]. For immunohistochemistry, randomly selected samples from different litters were applied. Sections were incubated with primary antibody against Ki-67 (Abcam, ab16667; 1:200), MUC2 (Servicebio, GB11344; 1:1000) or LRRC19 (Abcam, ab106657; 1:200) overnight at 4 °C. Next, sections were washed, incubated with a biotinylated secondary antibody and counterstained with 3, 3′-diaminobenzidine. Five random fields from ×200 images were viewed, and the expression of MUC2 and Ki-67 was analyzed by the absolute number of positively staining cells in well-orientated villi or crypts. Blinded reading of the histology was carried out by an experienced pathologist.

Periodic acid Schiff (PAS) staining

Randomly selected samples from different litters were applied for PAS staining. Colon slices were dewaxed, incubated with 1% periodic acid solution (Sigma-Aldrich, USA) for 10 min, stained by Schiff reagent (Sigma-Aldrich, USA) for 40 min and hematoxylin for 2–5 min. Each step was followed by rinsing in phosphate buffer saline. The number of positively stained particles in each crypt from five random fields in ×200 images was counted by an experienced pathologist in a blinded fashion to evaluate the presence of goblet cells.

Immunofluorescent staining

In order to evaluate the production and fucosylation of MUC2, immunofluorescence staining for $MUC2^+$ *Ulexeuropaeus* agglutinin I^+ ($UEA\text{-}I^+$) goblet cells were performed. Briefly, the deparaffinized sections were incubated with Antigen Unmasking Solution (Vector Laboratories, Inc., USA) for 15 min followed by 5% BSA to block non-specific binding. Subsequently, the colonic sections were incubated with primary antibody against MUC2 (Servicebio, GB11344; 1:1 000) overnight at 4 °C. Then the slices were washed three times with 1 × phosphate buffer saline for 5 min and incubated with fluorochrome-conjugated secondary antibody (Abbkine, A24421; 1:500) in the dark for 60 min followed by fluorescein isothiocyanate-conjugated UEA-I lectin (EY laboratories, inc., USA) for 30 min at room temperature. Nucleus was lastly dyed with DAPI (4, 6-diamidino-2-phenylindole). Fluorescence images were acquired with a Leika DM5000 B fluorescence microscope and five random fields from ×200 images were observed. For quantitative analysis, $MUC2^+UEA\text{-}I^+$ goblet cells in each well-orientated crypt were performed. Moreover, the small intestinal sections were incubated with primary antibody against IgA (Abcam, ab97231; 1:200) followed by secondary antibodies in the dark, and the IgA positive cells in each villus from five random fields in ×200 images were counted to quantitatively analyze the IgA level. Samples from different litters were randomly selected from each group for immunofluorescence staining. The quantitative analysis was performed in a blinded fashion by an experienced pathologist.

Realtime-PCR analysis

Small intestinal or colonic samples from different litters were randomly selected from each group for Realtime-PCR analysis. RNeasy mini kit (Qiagen, Germany), TIANScript RT Kit (TIANGEN, Inc., China), and Taqman Gene Expression Master Mix were used for RNA extraction, retrotranscription and quantitative PCR, respectively. Glyceraldehyde-3-phosphate dehydrogenase (GAPDH) mRNA expression was detected as internal control and the relative change in mRNA expression was calculated by $2^{-\Delta\Delta CT}$ method. All reactions were taken in triplicate. The oligonucleotide primer sequences (GENEWIZ, Inc., China) for target genes including *gapdh*, *Muc2*, and *Lrrc19* were as follows: *Gapdh*- forward:GGAGAAACCTGCCAAGTATG; *Gapdh*- reverse: TGGGAGTTGCTGTTGAAGTC; *Muc2*-forward: TCGCCCAAGTCGACACTCA; *Muc2*- reverse: GCAAATAGCCATAGTACAGTTACACAGC; *Lrrc19*- forwardCCCAGATGAGCTAAAGCACGA; *Lrrc19*- reverse: GAAAGCCCAGCTTTTCCCAAG.

Enzyme-linked immunosorbent assay (ELISA)

Samples from different litters were randomly selected from each group for ELISA. Collected colonic tissues were homogenized and centrifuged and then assessed by ELISA for IL-22 according to the tmanufacturer's instructions (SenBeiJia Biological Technology Co., Ltd., China). The content of IL-22 was quantified by measuring optical density from two to three titrations using standard curves.

Metagenomic sequencing and analysis

Randomly selected one frozen fecal sample from each litter of MCD and MHFD groups and all frozen fecal samples of WT-MHFD and $Lrrc19^{-/-}$-MHFD groups underwent metagenomic analysis (Realbio Genomics Institute, Shanghai, China). Briefly, the bacterial genomic DNA was extracted using QIAamp DNA Stool Mini Kit (Qiagen, Germany) based on the instruction manual. Then, DNA integrity and concentration were detected. Following the Illumina TruSeq DNA Sample Prep v2 Guide (Illumina, Inc., USA), the DNA paired-end libraries with an insert size of 500 bp were constructed and then the quality of all libraries was evaluated. All samples were subject to 150 bp paired-end sequencing on an Illumina HiSeq X Ten platform (Illumina, Inc., USA). Subsequently, the gut gene catalog was constructed, and open reading frames in contigs were predicted using MetaGeneMark (version 3.26). Clean reads were aligned to the microbial reference genomes downloaded from the National Center for Biological Information (NCBI, http://www.ncbi.nlm.nih.gov) using taxonomic and gene profiling SOAPalign2.21. Functional annotations were carried out by BLASTP search against the Kyoto Encyclopedia of Genes and Genomes (KEGG) database. For each functional feature (KO in KEGG database), its abundance was estimated by accumulating the relative abundance of all genes belonging to this feature.

Bray-Curtis metrics were used to calculate pairwise dissimilarities between samples and evaluate beta-diversity. The non-parametric Wilcoxon test was performed to calculate statistical significance of the gene, KO, diversity indices, and different taxonomic (phylum, genus, species) levels. Linear discriminant analysis (LDA) Effect Size (LEfSe) algorithm was used to identify the significantly different in relative abundance between groups, and different features with an LDA score cut-off of 2.0 and $P < 0.05$ were regarded as statistically significant.

Metabolomic analysis

The frozen fecal samples for metagenomic analysis were sent to the MetaboProfile Biotechnology (Shanghai, China) for metabolomic analysis. The samples were placed on an ice bath to thaw, 10 mg of feces were homogenized in 40 μL deionized water for 3 min, and then added with 160 μL methanol (with internal standard). After secondary homogenization for 3 min, the mixture was centrifuged at 18 000 g for 20 min at 10 °C and the supernatant was transferred to a new tube. Subsequently, 50 μL supernatant was added into a new 96-well plate with 50 μL deionized water, oscillated at 650 rpm for 10 min at 10 °C, waiting for further analysis. The tryptophan metabolites were detected by UPLC-MS/MS from the United States (ACQUITY UPLC-Xevo TQ-S, Waters Corp. USA). The raw data generated from UPLC-TQMS were analyzed by MassLynx of Waters (V4.1, Waters, USA), including peak extraction, integration, identification, and quantitative analysis for each metabolite.

Flow cytometry

The Peyer's patches and superficial adipose tissue were firstly removed from the colon. Then the colons were cut longitudinally, minced into small pieces and digested in the 1 mM EDTA followed by RPMI medium with 5% fetal bovine serum (FBS) and 0.15% collagenase II (275 U/mg)/0.05% dispase (1.1 U/mg) (Invitrogen) for 1 h at 37 °C to remove epithelial cells. Lymphocytes suspensions of lamina propria were prepared by sifting through 70 mm cell strainer and stained for further application. For intracellular staining, lamina propria lymphocytes (LPLs) were cultured and stimulated for 6 h with 50 ng/ml phorbol 12-myristate 13-acetate (PMA, Sigma) and 1 mg/ml ionomycin (Sigma) along with 10 ng/ml GolgiStop (BD Biosciences). For IL-22 induction, IL-23 (Peprotech) was applied. After incubation for 6 h, cells were washed in 1% serum PBS for three times, and surface antigen was stained with fluorescein isothiocyanate (FITC)- labeled Lin(CD3, CD19, GR1, Ly6C), peridinin-chlorophyll-protein complex (PerCP)- labeled CD45, phycoerythrin-Cyanine7 (PE-Cy7)- labeled CD127 antibody. Cells were then washed, fixed in Cytofix/Cytoperm, permeabilized with perm/wash buffer (BD Biosciences), and stained with allophycocyanin (APC)- labeled RORγt and phycoerythrin (PE)- labeled IL22 according to previously published protocols[63]. For flow cytometric analysis, ILC3s ($CD3^-CD19^-$ $GR1^-$ $Ly6C^-CD127^+CD45^+ROR\gamma t^+$ $IL\text{-}22^+$) were sorted with DxFLEX Beckman.

Statistics and reproducibility

Statistical analyses for all experiments except metagenomic analysis and metabolomic analysis were performed using GraphPad Prism software. Group sizes are described for each figure legend. All of our data first underwent normality testing to determine if they conform to a normal distribution. The measured data were presented as the means ± SDs and statistically analyzed by Student's *t* test in two groups or two-way analysis of variance (ANOVA) among four groups. A *P*- value less than 0.05 was considered statistically significant. We repeated each experiment at least three times. When sample size was reduced within a specific measurement, it represented a technical limitation due to insufficient plasma or tissue volume or equipment malfunction, etc. All tests were taken from distinct samples.

Reporting summary

Further information on research design is available in the Nature Portfolio Reporting Summary linked to this article.

Data availability

All authors had access to all data and reviewed and approved the final manuscript. All data are included in this article or uploaded as supplementary files. And metagenomic sequencing data have been deposited in NCBI(PRJNA703475). (http://www.ncbi.nlm.nih.gov/bioproject/703475; https://www.ncbi.nlm.nih.gov/sra/PRJNA703475). Supplementary Data 1 consists of the source data for the graphs in the main figures. Supplementary data 2 contains of the source data for metabolite detection.

Received: 17 March 2024; Accepted: 26 February 2025;
Published online: 12 March 2025

References

1. Gensollen, T., Iyer, S. S., Kasper, D. L. & Blumberg, R. S. How colonization by microbiota in early life shapes the immune system. *Science* **352**, 539–544 (2016).
2. Hornef, M. W. & Torow, N. 'Layered immunity' and the 'neonatal window of opportunity'—timed succession of non-redundant phases to establish mucosal host-microbial homeostasis after birth. *Immunology* **159**, 15–25 (2020).
3. Tamburini, S., Shen, N., Wu, H. C. & Clemente, J. C. The microbiome in early life: implications for health outcomes. *Nat. Med.* **22**, 713–722 (2016).
4. Macpherson, A. J., de Agüero, M. G. & Ganal-Vonarburg, S. C. How nutrition and the maternal microbiota shape the neonatal immune system. *Nat. Rev. Immunol.* **17**, 508–517 (2017).
5. Kimura, I. et al. Maternal gut microbiota in pregnancy influences offspring metabolic phenotype in mice. *Science* **367**, eaaw8429 (2020).
6. Oluwagbemigun, K. et al. Long-term dietary intake from infancy to late adolescence is associated with gut microbiota composition in young adulthood. *Am. J. Clin. Nutr.* **113**, 647–656 (2021).
7. Bolte, E. E., Moorshead, D. & Aagaard, K. M. Maternal and early life exposures and their potential to influence development of the microbiome. *Genome Med.* **14**, 4 (2022).
8. Chu, D. M. et al. The early infant gut microbiome varies in association with a maternal high-fat diet. *Genome Med.* **8**, 77 (2016).
9. Val-Laillet, D. et al. A maternal Western diet during gestation and lactation modifies offspring's microbiota activity, blood lipid levels, cognitive responses, and hippocampal neurogenesis in Yucatan pigs. *FASEB J.* **31**, 2037–2049 (2017).
10. Lippert, R. N. et al. Maternal high-fat diet during lactation reprograms the dopaminergic circuitry in mice. *J. Clin. Invest.* **130**, 3761–3776 (2020).
11. Xie, R. et al. Maternal High Fat Diet Alters Gut Microbiota of Offspring and Exacerbates DSS-Induced Colitis in Adulthood. *Front. Immunol.* **9**, 2608 (2018).
12. Burgueño, J. F. & Abreu, M. T. Epithelial Toll-like receptors and their role in gut homeostasis and disease. *Nat. Rev. Gastroenterol. Hepatol.* **17**, 263–278 (2020).
13. Fulde, M. et al. Neonatal selection by Toll-like receptor 5 influences long-term gut microbiota composition. *Nature* **560**, 489–493 (2018).
14. Lu, P. et al. Intestinal epithelial Toll-like receptor 4 prevents metabolic syndrome by regulating interactions between microbes and intestinal epithelial cells in mice. *Mucosal Immunol.* **11**, 727–740 (2018).
15. Chai, L. et al. LRRC19, a novel member of the leucine-rich repeat protein family, activates NF-kappaB and induces expression of proinflammatory cytokines. *Biochem. Biophys. Res. Commun.* **388**, 543–548 (2009).
16. Su, X. et al. LRRC19 expressed in the kidney induces TRAF2/6-mediated signals to prevent infection by uropathogenic bacteria. *Nat. Commun.* **5**, 4434 (2014).
17. Cao, S. et al. The Gut Epithelial Receptor LRRC19 Promotes the Recruitment of Immune Cells and Gut Inflammation. *Cell Rep.* **14**, 695–707 (2016).
18. Martens, E. C., Neumann, M. & Desai, M. S. Interactions of commensal and pathogenic microorganisms with the intestinal mucosal barrier. *Nat. Rev. Microbiol.* **16**, 457–470 (2018).
19. Kayama, H., Okumura, R. & Takeda, K. Interaction between the microbiota, epithelia, and immune cells in the intestine. *Annu. Rev. Immunol.* **38**, 23–48 (2020).
20. Martel, J. et al. Gut barrier disruption and chronic disease. *Trends Endocrinol. Metab.* **33**, 247–265 (2022).

21. Breugelmans, T. et al. The role of mucins in gastrointestinal barrier function during health and disease. *Lancet Gastroenterol. Hepatol.* **7**, 455–471 (2022).
22. Garrett, W. S. Immune recognition of microbial metabolites. *Nat. Rev. Immunol.* **20**, 91–92 (2020).
23. Kayama, H. & Takeda, K. Manipulation of epithelial integrity and mucosal immunity by host and microbiota-derived metabolites. *Eur. J. Immunol.* **50**, 921–931 (2020).
24. Su, X. et al. LRRC19 Promotes Permeability of the Gut Epithelial Barrier Through Degrading PKC-ζ and PKCι/λ to Reduce Expression of ZO1, ZO3, and Occludin. *Inflamm. Bowel Dis.* **27**, 1302–1315 (2021).
25. Birchenough, G. M., Johansson, M. E., Gustafsson, J. K., Bergström, J. H. & Hansson, G. C. New developments in goblet cell mucus secretion and function. *Mucosal Immunol.* **8**, 712–719 (2015).
26. Mathias, A., Pais, B., Favre, L., Benyacoub, J. & Corthésy, B. Role of secretory IgA in the mucosal sensing of commensal bacteria. *Gut Microbes* **5**, 688–695 (2014).
27. Scott, S. A., Fu, J. & Chang, P. V. Microbial tryptophan metabolites regulate gut barrier function via the aryl hydrocarbon receptor. *Proc. Natl Acad. Sci. USA* **117**, 19376–19387 (2020).
28. Wang, Y. et al. Modulation of tryptophan metabolism via AHR-IL22 pathway mediates the alleviation of DSS-induced colitis by chitooligosaccharides with different degrees of polymerization. *Carbohydr. Polym.* **319**, 121180 (2023).
29. Patnaude, L. et al. Mechanisms and regulation of IL-22-mediated intestinal epithelial homeostasis and repair. *Life Sci.* **271**, 119195 (2021).
30. Nyangahu, D. D. et al. Disruption of maternal gut microbiota during gestation alters offspring microbiota and immunity. *Microbiome* **6**, 124 (2018).
31. Paone, P. & Cani, P. D. Mucus barrier, mucins and gut microbiota: the expected slimy partners. *Gut* **69**, 2232–2243 (2020).
32. Bergstrom, K. et al. Proximal colon-derived O-glycosylated mucus encapsulates and modulates the microbiota. *Science* **370**, 467–472 (2020).
33. Pham, T. A. et al. Epithelial IL-22RA1-mediated fucosylation promotes intestinal colonization resistance to an opportunistic pathogen. *Cell Host Microbe* **16**, 504–516 (2014).
34. Cai, R. et al. Interactions of commensal and pathogenic microorganisms with the mucus layer in the colon. *Gut Microbes* **11**, 680–690 (2020).
35. Schroeder, B. O. et al. Bifidobacteria or fiber protects against diet-induced microbiota-mediated colonic mucus deterioration. *Cell Host Microbe* **23**, 27–40.e7 (2018).
36. Rohr, M. W., Narasimhulu, C. A., Rudeski-Rohr, T. A. & Parthasarathy, S. Negative effects of a high-fat diet on intestinal permeability: a review. *Adv. Nutr.* **11**, 77–91 (2020).
37. Gohir, W. et al. High-fat diet intake modulates maternal intestinal adaptations to pregnancy and results in placental hypoxia, as well as altered fetal gut barrier proteins and immune markers. *J. Physiol.* **597**, 3029–3051 (2019).
38. Ma, J. et al. High-fat maternal diet during pregnancy persistently alters the offspring microbiome in a primate model. *Nat. Commun.* **5**, 3889 (2014).
39. Devlin, A. S. et al. Modulation of a Circulating Uremic Solute via Rational Genetic Manipulation of the Gut Microbiota. *Cell Host Microbe* **20**, 709–715 (2016).
40. Jabs, S. et al. Impact of the gut microbiota on the m(6)A epitranscriptome of mouse cecum and liver. *Nat. Commun.* **11**, 1344 (2020).
41. Gentile, C. L. & Weir, T. L. The gut microbiota at the intersection of diet and human health. *Science* **362**, 776–780 (2018).
42. Chassaing, B. et al. Dietary emulsifiers impact the mouse gut microbiota promoting colitis and metabolic syndrome. *Nature* **519**, 92–96 (2015).
43. Zhang, X. et al. Dietary cholesterol drives fatty liver-associated liver cancer by modulating gut microbiota and metabolites. *Gut* **70**, 761–774 (2021).
44. Parada Venegas, D. et al. Short Chain Fatty Acids (SCFAs)-Mediated Gut Epithelial and Immune Regulation and Its Relevance for Inflammatory Bowel Diseases. *Front. Immunol.* **10**, 277 (2019).
45. Yang, W. et al. Intestinal microbiota-derived short-chain fatty acids regulation of immune cell IL-22 production and gut immunity. *Nat. Commun.* **11**, 4457 (2020).
46. Lavelle, A. & Sokol, H. Gut microbiota-derived metabolites as key actors in inflammatory bowel disease. *Nat. Rev. Gastroenterol. Hepatol.* **17**, 223–237 (2020).
47. Sun, M., Ma, N., He, T., Johnston, L. J. & Ma, X. Tryptophan (Trp) modulates gut homeostasis via aryl hydrocarbon receptor (AhR). *Crit. Rev. Food Sci. Nutr.* **60**, 1760–1768 (2020).
48. Dong, F. & Perdew, G. H. The aryl hydrocarbon receptor as a mediator of host-microbiota interplay. *Gut Microbes* **12**, 1859812 (2020).
49. Zhang, J. et al. Metabolites of microbiota response to tryptophan and intestinal mucosal immunity: A therapeutic target to control intestinal inflammation. *Med Res Rev.* **41**, 1061–1088 (2021).
50. Xie, W. et al. A bovine lactoferricin-lactoferrampin-encoding Lactobacillus reuteri CO21 regulates the intestinal mucosal immunity and enhances the protection of piglets against enterotoxigenic Escherichia coli K88 challenge. *Gut Microbes* **13**, 1956281 (2021).
51. Wang, G. et al. Microbiota-derived indoles alleviate intestinal inflammation and modulate microbiome by microbial cross-feeding. *Microbiome* **12**, 59 (2024).
52. Zelante, T. et al. Tryptophan catabolites from microbiota engage aryl hydrocarbon receptor and balance mucosal reactivity via interleukin-22. *Immunity* **39**, 372–385 (2013).
53. Wlodarska, M. et al. Indoleacrylic Acid Produced by Commensal Peptostreptococcus Species Suppresses Inflammation. *Cell Host Microbe* **22**, 25–37.e6 (2017).
54. Dong, F. et al. Intestinal microbiota-derived tryptophan metabolites are predictive of Ah receptor activity. *Gut Microbes* **12**, 1–24 (2020).
55. Keir, M., Yi, Y., Lu, T. & Ghilardi, N. The role of IL-22 in intestinal health and disease. *J. Exp. Med.* **217**, e20192195 (2020).
56. Goto, Y. et al. Innate lymphoid cells regulate intestinal epithelial cell glycosylation. *Science* **345**, 1254009 (2014).
57. Engevik, M. A. et al. Bifidobacterium dentium fortifies the intestinal mucus layer via autophagy and calcium signaling pathways. *mBio* **10**, e01087–19 (2019).
58. Sgritta, M. et al. Mechanisms underlying microbial-mediated changes in social behavior in mouse models of autism spectrum disorder. *Neuron* **101**, 246–259.e6 (2019).
59. Mu, Q., Tavella, V. J. & Luo, X. M. Role of Lactobacillus reuteri in human health and diseases. *Front Microbiol* **9**, 757 (2018).
60. Wu, H. et al. Lactobacillus reuteri maintains intestinal epithelial regeneration and repairs damaged intestinal mucosa. *Gut Microbes* **11**, 997–1014 (2020).
61. Hou, Q. et al. Lactobacillus accelerates ISCs regeneration to protect the integrity of intestinal mucosa through activation of STAT3 signaling pathway induced by LPLs secretion of IL-22. *Cell Death Differ.* **25**, 1657–1670 (2018).
62. Kumar, N. et al. A YY1-dependent increase in aerobic metabolism is indispensable for intestinal organogenesis. *Development* **143**, 3711–3722 (2016).
63. Liang, Z. et al. Intestinal CXCR6(+) ILC3s migrate to the kidney and exacerbate renal fibrosis via IL-23 receptor signaling enhanced by PD-1 expression. *Immunity* **57**, 1306–1323.e8 (2024).

Acknowledgements
The authors thank the other participants of this work. This research is supported by the grants from the National Natural Science Foundation of China (82470569, 82270574, 82400632, and 81970488), Beijing-Tianjin-Hebei Basic Research Cooperation Project (23JCZXJC00200) and Guangzhou Basic and Applied Basic Research Project, (SL2024A04J02246).

Author contributions
Y.S., S.M.H., B.M.W., X.M.S., and H.L.C. were involved in the study design; Y.S., S.M.H., M.F.L., Y.W.Y., J.H.M., R.X.X., J.Y.W., Q.J.Z., S.Q.Q., L.L.H., J.Y.J., Q.Z., X.L., H.H., Y.Z.Y., J.M.W., and G.J. performed the experiments; Y.S., S.M.H., M.F.L., Y.W.Y., R.X.X., Y.Z.Y., W.T.L., R.C.Y., and H.L.C. analyzed the data; Y.S., S.M.H., M.F.L., Y.W.Y., and H.L.C. wrote the manuscript; HLC and XMS made the critical revision. All authors who contributed to the design and writing of the paper agreed with the final version of the content of the manuscript.

Competing interests
The authors declare no competing interests.

Additional information
Supplementary information The online version contains supplementary material available at https://doi.org/10.1038/s42003-025-07836-z.

Correspondence and requests for materials should be addressed to Xiaomin Su or Hailong Cao.

Peer review information *Communications Biology* thanks Chien-Wen Su and the other, anonymous, reviewer(s) for their contribution to the peer review of this work. Primary Handling Editor: Christina Karlsson Rosenthal.